

## Intraseasonal variability of terrestrial biospheric CO<sub>2</sub> fluxes over India during summer monsoons.

Vinu Valsala,<sup>1</sup> Yogesh K. Tiwari,<sup>1</sup> Prasanth Pillai,<sup>1</sup> Mathew Roxy,<sup>1</sup> Shamil Maksyutov,<sup>2</sup> and Raghu Murtugudde<sup>3</sup>

Received 3 August 2012; revised 29 January 2013; accepted 31 January 2013.

[1] The intraseasonal oscillations (ISOs) in terrestrial biospheric fluxes of carbondioxide (CO<sub>2</sub>) over the Indian subcontinent were investigated for the summer monsoon season from June to September. We utilized two optimized datasets of Net Ecosystem Exchange (NEE) fluxes of CO<sub>2</sub> at a spatial resolution of 1° × 1° grid and at daily time scale for the years 2000–2009. Seasonally, over the whole of Indian subcontinent, terrestrial biospheric CO<sub>2</sub> fluxes were found to be a net source (sink) during June and July (August and September). Intraseasonal variability of CO<sub>2</sub> fluxes for the two distinct time scales, 30–60 days and 10–20 days, was extracted with a spectral harmonic filter. The dominant ISO mode in the CO<sub>2</sub> flux over India is at a period of 60 days or longer during weak monsoons years but at 10–30 days for strong monsoon years. The ISOs of CO<sub>2</sub> flux show coherent structures along with corresponding rainfall ISOs at a 2–3 day lag (CO<sub>2</sub> lags rainfall) and nearly 3–4 day lag with ISOs in surface air-temperature (CO<sub>2</sub> lags air-temperature). The ranges of these lags are consistent in the two data products examined here. The apparent lags between CO<sub>2</sub> flux and rainfall ISOs are found to be induced by the temperature effects on net primary production (NPP) and ecosystem respiration (RE). The terrestrial biospheric fluxes over the subcontinent are coherent with the northward propagating summer monsoon ISOs albeit as a combination of rainfall, available radiation, and air-temperature. The study offers a mechanistic understanding of variability of terrestrial biospheric sources and sinks of CO<sub>2</sub> over the Indian subcontinent, in tandem with the intraseasonal variability of the summer monsoon rainfall.

**Citation:** Valsala, V., Y. K. Tiwari, P. Pillai, M. Roxy, S. Maksyutov, and R. Murtugudde (2013), Intraseasonal variability of terrestrial biospheric CO<sub>2</sub> fluxes over India during summer monsoons, *J. Geophys. Res. Biogeosci.*, 118, doi:10.1002/jgrg.20037.

### 1. Introduction

[2] The Indian Summer Monsoon Rainfall (hereinafter referred to as monsoon rainfall) between June and September contributes to about 80–90% of the annual mean rainfall over the Indian subcontinent [Mooley and Shukla, 1987; Mooely and Parthasarathy, 1984; Parthasarathy, 1984]. It has tremendous influence on the agricultural yield and hence, the economic development of the country [Gadgil and Rupa Kumar, 2006; Preethi and Revadekar, 2012]. As for the terrestrial ecosystems, the wet monsoon during June to late September demarcates the boundary between generally hot and dry seasons for the plants during the pre-monsoon from April to May and the relatively dry and cool season from November onward. During the summer monsoon season, the terrestrial ecosystem of the subcontinent responds to the monsoonal precipitation which nurtures

biospheric growth that peaks in September and October (see NDVI climatological seasonal cycle over the Indian region from Figure 1).

[3] The monsoon rainfall comprises frequently occurring wet and dry spells of precipitation generally over a cycle of 10–90 days but have two preferred bands of variability with periods ranging from 10 to 20 days [Krishnamurti and Ardanuy, 1980] and 20 to 60 days [Murakami *et al.*, 1984; Krishnamurti and Subrahmanyam, 1982; Lau and Peng, 1987]. These wet and dry spells of monsoon rainfall denote the intraseasonal variability of the summer monsoon season. The intraseasonal variability with 20–60 day time scale exhibits a northward and eastward propagation [Yasunari, 1979, 1980; Sikka and Gadgil, 1980] while that with the 10–20 day time scale is either stationary or propagates northward, with a prominent westward propagation over the monsoon region [Goswami and Ajayamohan, 2001]. The present study deals with the Indian subcontinental terrestrial biospheric CO<sub>2</sub> flux variability associated with these two distinctively propagating oscillations of 10–20 day and 30–60 day periodicities in rainfall, hereinafter collectively referred to as Intraseasonal Oscillations (ISOs).

[4] The hypothesis of a possible connection between the high-frequency oscillations of terrestrial biospheric CO<sub>2</sub> fluxes over the Indian subcontinent with the corresponding

<sup>1</sup>Indian Institute of Tropical Meteorology, Pune, India.

<sup>2</sup>National Institute for Environmental Studies, Tsukuba, Japan.

<sup>3</sup>ESSIC, University of Maryland, College Park, Maryland, USA.

Corresponding author: V. Valsala, Indian Institute of Tropical Meteorology, Pune, Maharashtra 411008, India. (valsala@tropmet.res.in)

©2013. American Geophysical Union. All Rights Reserved.  
2169-8953/13/10.1002/jgrg.20037

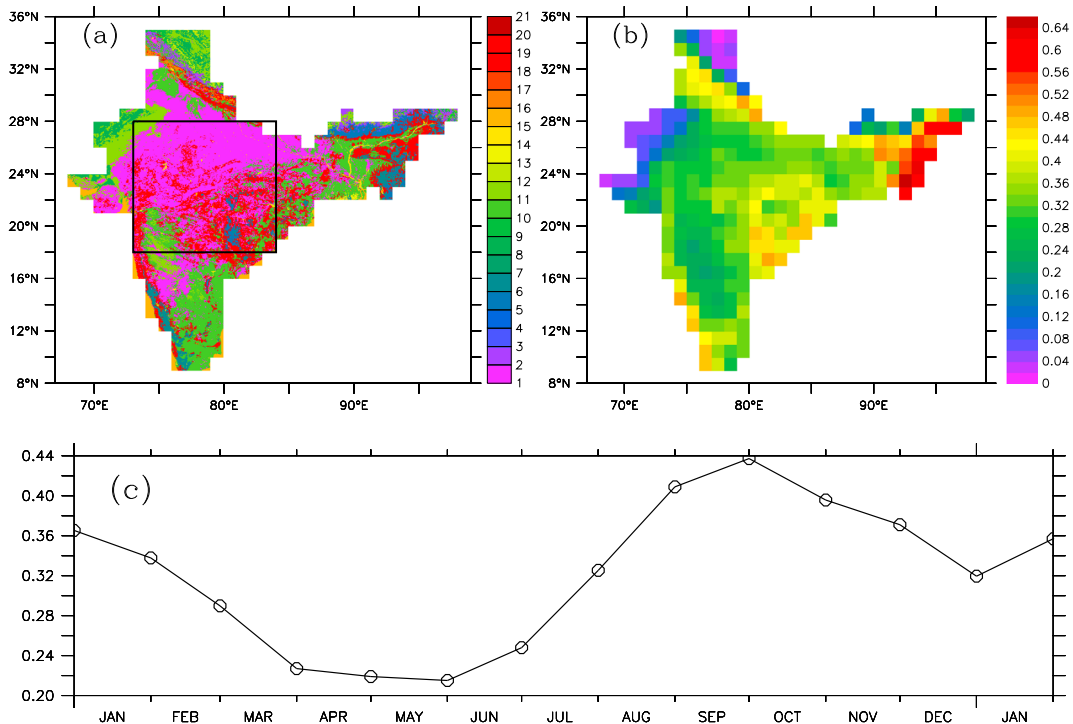


**Figure 1.** (a) Annual land use data over India from Global Land Cover Characterization (GLCC) data sets as derived from the 1 km Advanced Very High Resolution Radiometer (AVHRR) data spanning April 1992 to March 1993. The vegetation types are defined by biosphere atmosphere transfer scheme (BATS). The 20 vegetation types shown here are (1) crop/mixed farming, (2) short grass, (3) evergreen needle leaf tree, (4) deciduous needle leaf tree, (5) deciduous broad leaf tree, (6) evergreen broad leaf tree, (7) tall grass, (8) desert, (9) tundra, (10) irrigated crop, (11) semi-desert, (12) ice cap/glacier, (13) bog or marsh, (14) inland water, (15) ocean, (16) evergreen shrub, (17) deciduous shrub, (18) mixed woodland, (19) forest/field mosaic, and (20) water and land mixture. (b) Annual mean normalized difference vegetation index (NDVI) obtained from 1982 to 2000 satellite data. (c) The seasonal cycle of climatological NDVI over Indian subcontinent. The red line indicates the data from *Niwa et al.* [2012] but the amplitude is scaled by half.

oscillations of monsoonal precipitation is logical because the ecosystem is strongly influenced by the fluctuations in rainfall and temperature [Wu *et al.*, 2011]. The background temperature during the summer monsoon is favorable for the tropical plants to grow. However, the relationship between rainfall, temperature, and photosynthesis can be further complicated during prolonged rainfall spells which leads to decreased solar insolation, impacting the photosynthetically active radiation (PAR), and thereby inhibiting photosynthesis and net primary production (NPP) of the terrestrial ecosystem. The soil moisture and runoff of precipitated water may offer confounding complications with the ISOs and PAR variability. Therefore, intrinsic interactions of various components which can influence the ecosystem may also modulate NPP, net ecosystem exchange (NEE), and biosphere respiration (RE) [Braswell, *et al.*, 1997; Xu *et al.*, 2004].

[5] Several prior studies have investigated the connection between Indian biospheric CO<sub>2</sub> fluxes and monsoon rainfall by modeling them, but generally with less attention to the monsoon ISO and its variability. For example, *Tian et al.* [2003] examined the interannual variability of NPP and NEE over Asian region. *Nayak et al.* [2013, 2010] focused specifically on the interannual variability of NPP over India from 1981 to 2006 using model simulations. They used the CASA model of *Potter et al.* [2003] and calculated

NPP from light use efficiency (LUE) scaled by stress vectors dependent on temperatures and soil moisture. The study identified that the country's annual mean NPP is strongly correlated with the rainfall variability but only weakly correlated with temperature variability on interannual time scales. This suggests that process modeling of primary production over the Indian subcontinent is highly sensitive to rainfall during the summer monsoon. The study also pointed out that the interannual variability of NPP over India is largest over the low productivity regions (mixed shrub, grassland), moderate over the agricultural regions, and relatively small over the forest regions. They also noticed that NPP growth rate over the country declined with a corresponding increase in the growth rate of global atmospheric CO<sub>2</sub> and thus implying a potential role for the regional terrestrial ecosystem in the global carbon cycle. Our study is clearly distinct from these previous studies in its attempt to investigate the intraseasonal variability of Indian terrestrial biospheric CO<sub>2</sub> fluxes during summer monsoon.

[6] The examination of terrestrial biospheric fluxes of CO<sub>2</sub> over India is important for estimating the country's net biospheric sinks of this greenhouse gas. The carbon pool for the Indian forests is estimated to be 2026.72 Mt for the year 1995 [Lal and Singh, 2000]. Estimates of annual

carbon uptake increment suggest that the country's forests and plantations have been able to remove at least 0.125 petagram carbon (Pg C) from the atmosphere in the year 1995. Assuming that the present forest cover in India will sustain itself with a marginal annual increase by 0.5 million hectares in areas of plantations, we can expect the forests to continue to act as a net carbon sink in the future [*Lal and Singh, 2000*]. According to the India State of Forest Report (ISFR) prepared by the Forest Survey of India, Ministry of Environment and Forest, Government of India, the status of total forest cover in India is 675,538 km<sup>2</sup> in 2001, 678,333 km<sup>2</sup> in 2003, 690,899 km<sup>2</sup> in 2009, and 692,027 km<sup>2</sup> in 2011, bringing the forest cover up to 21.05% of geographical area of India [*ISFR, 2011*].

[7] The motivation for examining the high-frequency oscillations of terrestrial biospheric CO<sub>2</sub> fluxes in response to monsoon ISOs can be viewed as follows. The global net sink of CO<sub>2</sub> by the terrestrial biosphere is estimated to be nearly 2 Pg C per year which is approximately one quarter of the annual mean fossil fuel emissions [*Gurney et al., 2004; Raupach, 2011*]. Although this net sink appears relatively small, the seasonal amplitude of CO<sub>2</sub> sources and sinks themselves is on the order of a few tens of petagram carbon. A delicate balance between the net source and sink is thus very important in determining the global budget of annual mean sink of atmospheric CO<sub>2</sub> [*Canadell et al., 2007*]. This can equally well be illustrated at regional scales; for example, based on the data used in this study, the area-integrated terrestrial biospheric CO<sub>2</sub> fluxes over India have seasonal amplitude of 1.0 Pg C during June to -1.0 Pg C during September (positive flux corresponds to a net emission), eliciting that these seasonal amplitudes are roughly on the order of global net sink of terrestrial biosphere which itself is nearly 2 Pg C yr<sup>-1</sup>. Therefore, the intricate balance between seasonal sources and sinks of regional CO<sub>2</sub> is indeed critical in maintaining the global average. Any variability of this seasonal cycle (in the present context we refer to the intraseasonal variability) of CO<sub>2</sub> is also important in determining the net annual mean. The response of the monsoon intraseasonal variability to global warming and the consequent response of the regional sources/sinks cannot be evaluated without a baseline study of the CO<sub>2</sub> flux variability at ISO time scales such as the one we present here.

[8] The net terrestrial biospheric CO<sub>2</sub> fluxes over the Indian region during the summer monsoon season exhibit a transition from a source during June to a sink during September. The abundant rain water during the August–September season causes the ecosystem to exceed its NPP over NEE and respiration in terms of CO<sub>2</sub> emission. We note from observational analysis that (as shown in later sections) the high-frequency variability is larger during June and September. Our further analysis in this direction reveals that India's terrestrial biospheric fluxes of CO<sub>2</sub> exhibit large scale (organized) intraseasonal variability in tandem with ISOs of monsoon rainfall.

[9] The following are the major questions addressed in this paper: (a) Do the terrestrial biospheric CO<sub>2</sub> fluxes over India exhibit any significant intraseasonal oscillations associated with the variability of monsoon rainfall? (b) How is the ISO of terrestrial CO<sub>2</sub> flux determined? (c) What is its contribution to the annual mean sources and sinks of biospheric CO<sub>2</sub> over

**Table 1.** Acronyms Used in the Text and Their Expansions

ISO	Intraseasonal Oscillation
NEE	Net Ecosystem Exchange
NPP	Net Primary Production
GPP	Gross Primary Production
RE	Respiration
NDVI	Normalized Difference Vegetation Index
CT	CarbonTracker
VISIT	Vegetation Integrative Simulator for Trace gases
LUE	Light Use Efficiency
AVHRR	Advanced Very High Resolution Radiometer

the Indian continent? The rest of the paper is organized as follows. Section 2 describes data and methods used in this study. Section 3 presents the results and a discussion is offered in section 4. The paper is summarized in section 5. A table with list of common acronyms used in the text is provided in Table 1.

## 2. Data and Methods

### 2.1. Net Ecosystem Exchange (NEE) Data From Carbon Tracker

[10] We use the terrestrial biospheric CO<sub>2</sub> flux data from the optimized data set provided by the Carbon Tracker (CT) which is developed and maintained by the Earth System Research Laboratory (ESRL) at National Oceanographic and Atmospheric Administration (NOAA) [*Peters et al, 2007*]. The CT version 2010 is used in this study. This data set provides optimized terrestrial biospheric CO<sub>2</sub> flux estimates at spatial resolution of 1° × 1° horizontal grids and a temporal resolution of three hourly time steps from year 2000 to 2009. This data set is produced by an ensemble simulation and assimilation of global observations of atmospheric concentrations of CO<sub>2</sub> in a transport model. The CT ensemble data assimilation assumes that the four surface flux modules (terrestrial biosphere, ocean, fossil fuel, and forest fire emission) drive the instantaneous atmospheric CO<sub>2</sub> concentrations. The combination fluxes used in CT can be expressed as

$$F(x, y, t) = \lambda F_{\text{bio}}(x, y, t) + \lambda F_{\text{oce}}(x, y, t) + F_{\text{ff}}(x, y, t) + F_{\text{fire}}(x, y, t) \quad (1)$$

[11] where,  $F_{\text{bio}}$ ,  $F_{\text{oce}}$ ,  $F_{\text{ff}}$  and  $F_{\text{fire}}$  represent the biospheric, oceanic, fossil fuel, and forest fire emissions of CO<sub>2</sub>.  $\lambda$  represents a set of linear scaling factors applied to the fluxes and is estimated in the assimilation methodology. These scaling factors are the final product of the assimilation and together with the prior fluxes form the optimized estimate of CO<sub>2</sub> fluxes.  $\lambda$  is estimated for each week during the assimilation and assumed constant over this period. The scaling factor  $\lambda$  is spatially divided into 11 discrete land regions over the global domain. Furthermore, the terrestrial biosphere is also divided up according to ecosystem types as well as the geographical location. Thereafter, each of the 11 land regions contains a maximum of 19 ecosystem types (see CT documentation at <http://www.esrl.noaa.gov/gmd/ccgg/carbontracker/tu-torial.html> for more details).

[12] Since the correction to the fluxes is applied only on a weekly basis, by way of optimizing the  $\lambda$  in the CT assimilation, any variability below this period is solely

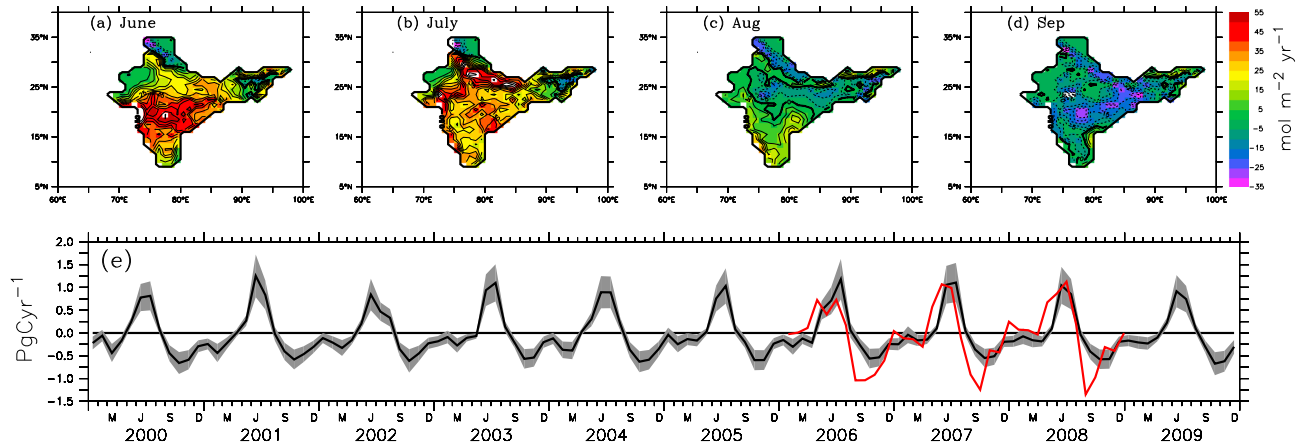


**Figure 2.** Monthly mean CO<sub>2</sub> fluxes over continental India during (a) June, (b) July, (c) August, and (d) September derived for 2000 to 2009 from CT data are shown. The anomalous years 2002 and 2004 are not included in the mean. The transition of CO<sub>2</sub> source to sink during summer monsoon rainfall is highlighted in Figures 1a–1d. Positive values show CO<sub>2</sub> sources. Units are in mol m<sup>-2</sup>yr<sup>-1</sup>. (e) Seasonal cycle (line) and daily standard deviations during each month (shades) of area-integrated land-air CO<sub>2</sub> fluxes from 2000 to 2009.

introduced from the prior fluxes. However, here we offer a caveat that there are no CO<sub>2</sub> measurements from the Indian subcontinent itself that went into constraining the terrestrial biospheric flux priors used in the CT. Therefore, the retrieved NEE fluxes over India are constrained where possible by similar eco-regions north of the Himalayas in Kazakhstan, Russia, China, and Korea, and also Indonesia for a small part of India that falls in the Tropical Asia Transcom domain [Peters *et al.*, 2007]. Since the CT inversion scheme does not have the atmospheric CO<sub>2</sub> data sampled within the Indian subcontinent, the reliability of optimized NEE largely depends on the reliability of prior fluxes used. Therefore, in the following, we document the prior fluxes used in CT.

[13] The biosphere model used to produce the prior fluxes in the CT is the Carnegie-Ames-Stanford-Approach (CASA) biogeochemical model. The version of CASA used in CT is that of van der Werf *et al.* [2003, 2006]. This is basically an adaptation of CASA model of the 1990s which are documented in Potter *et al.* [2003], Field *et al.* [1995], and Randerson *et al.* [1996]. In the work of van der Werf

*et al.* [2003], the above CASA model has been modified to account for NEE changes due to fire events. The simulated CASA used in the prior fluxes of CT thus has impact of fires both as a reduction in biomass due to fire events and changes in carbon emissions due to the bacterial decay upon the mortality of vegetation (but not completely burned) during fire.

[14] The model was run using input from meteorological parameters (taken from ECMWF re-analysis) to drive biophysical processes, as well as satellite observed Normalized Difference Vegetation Index (NDVI) to track plant phenology. The NDVI data were taken from AVHRR NDVI. The CASA model was driven by year specific weather and satellite observations, including the effects of fires on photosynthesis and respiration. This simulation gives 1° × 1° grid global fluxes on a monthly time resolution.

[15] The Net Ecosystem Exchange (NEE) is computed from the monthly mean CASA Net Primary Production (NPP) and ecosystem respiration (RE) outputs. Higher frequency variations (diurnal and synoptic) are added to Gross Primary

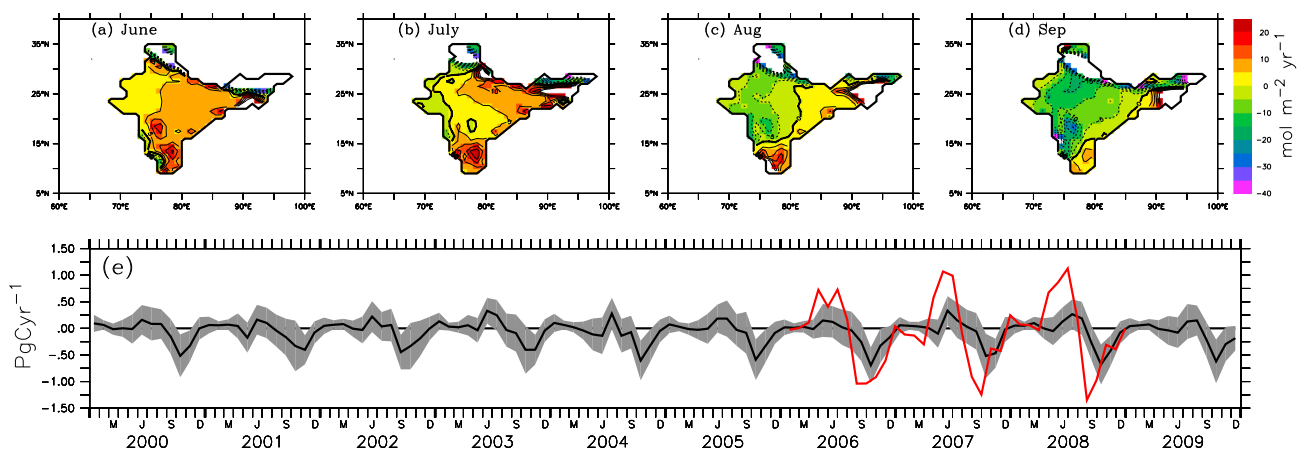


**Figure 3.** Same as Figure 2 but from VISIT data.

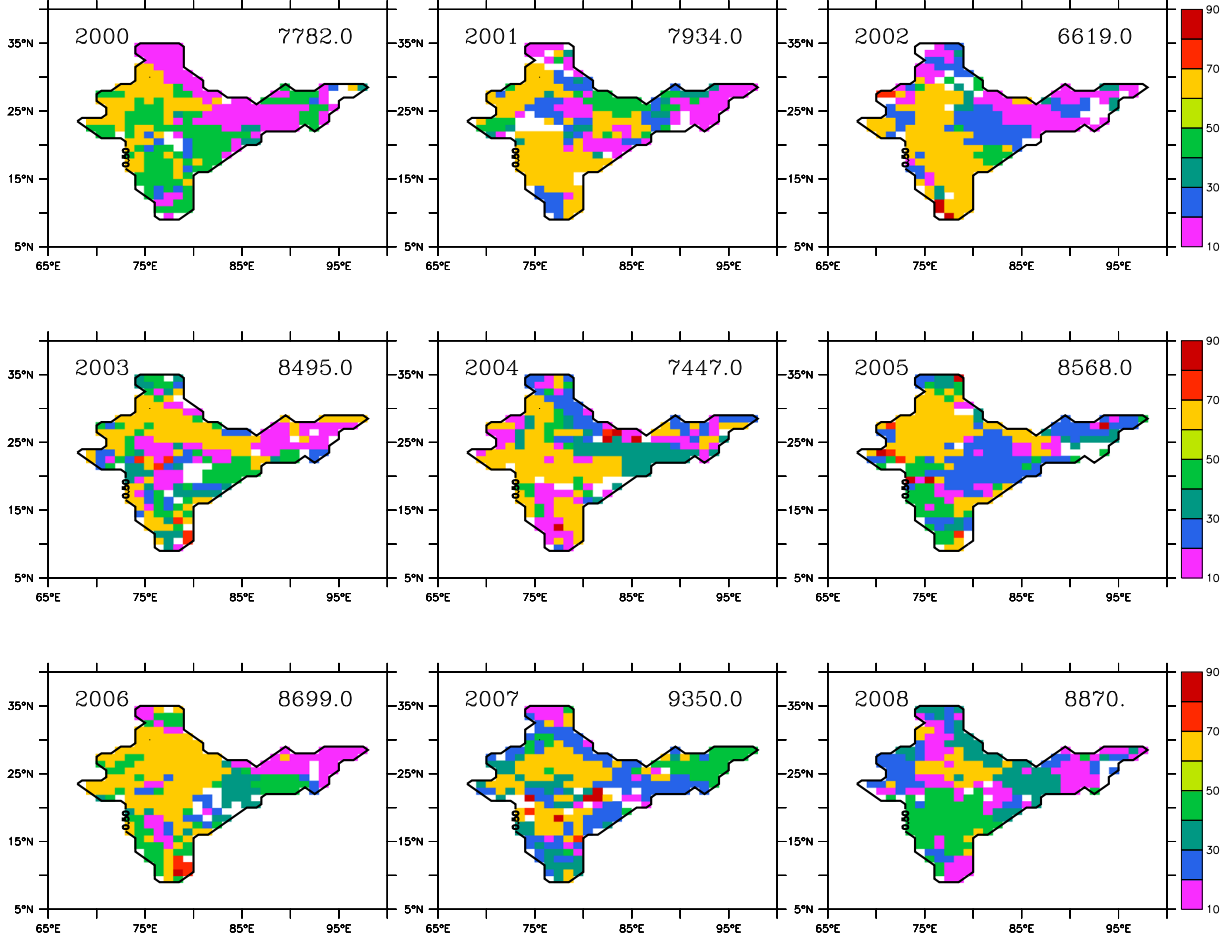


**Figure 4.** Spatial pattern of periodicity (in days) of maximum power of variability of daily fluxes for the four summer monsoon months from June to September. Patterns are shown for each year separately. The annual mean rainfall for each year is shown on top right of each panel.

Production (obtained as  $GPP = 2 \times NPP$ ) and RE (obtained as  $RE = NE - GPP$ ) fluxes every 3 h using a simple temperature  $Q_{10}$  (refer equation (5)) relationship assuming a global  $Q_{10}$  value of 1.5 for respiration and a linear scaling of photosynthesis with solar radiation. Instantaneous NEE for each 3 h interval is thus created as

$$NEE_{(t)} = GPP_{(t,t)} + RE_{(T,t)} \quad (2)$$

$$GPP_{(t)} = I_{(t)} \left( \frac{\sum GPP}{\sum I} \right) \quad (3)$$

$$RE_{(t)} = Q_{10(t)} \left( \frac{\sum RE}{\sum Q_{10}} \right) \quad (4)$$

$$Q_{10(t)} = 1.5 \left[ \frac{(T_{2m} - T_0)}{10.0} \right] \quad (5)$$

[16] where  $T = 2$  m temperature,  $I =$  incoming solar radiation,  $t =$  time, and summations are done over 1 month, for each grid box [Peters *et al.*, 2007]. There is no separation of RE on autotrophic and heterotrophic level at synoptic and hourly scales. Therefore, the sudden surges of RE with rain events (as observed in the tropical forests by Xu *et al.* [2004]) may be only empirically represented with corresponding changes in air-temperature and solar insulations. But RE surges occur only in the first rain burst but not in the subsequent rain events. This is perhaps not represented in CT.

[17] It should be noted that the GPP and RE are simulated in CASA only on monthly time scales and the NEE data at three-hourly time resolution within each month is estimated using the simple relation described above. However, the NEE was corrected on a weekly basis in the assimilation. Therefore the NEE data can represent signatures on ISO time scales (7 days or longer) more realistically and they are not simply arising from the relations shown above. Here, we reemphasize that there are no CO<sub>2</sub> measurements from the Indian subcontinent itself that help to constrain CASA's biospheric flux priors in the CT. One may argue that the weekly optimization of CASA NEE using inversions of atmospheric CO<sub>2</sub> in CT system is barely affecting the priors because of this lack of data from the Indian subcontinent. Nevertheless, a trajectory analysis shows that sensitivity of Indian landmass CO<sub>2</sub> emissions can be sensed at far distances as a result of the monsoon dynamics [Tiwari *et al.*, 2013].

## 2.2. Net Ecosystem Exchange (NEE) From Optimized Visit Model

[18] Vegetation Integrative Simulator for Trace gases (VISIT) is a prognostic biosphere model [Ito, 2010]. Global vegetation types are classified into 15 biomes in this model and they are inferred based on the maps of MODIS land cover data [Friedl *et al.*, 2002]. The meteorological reanalysis data

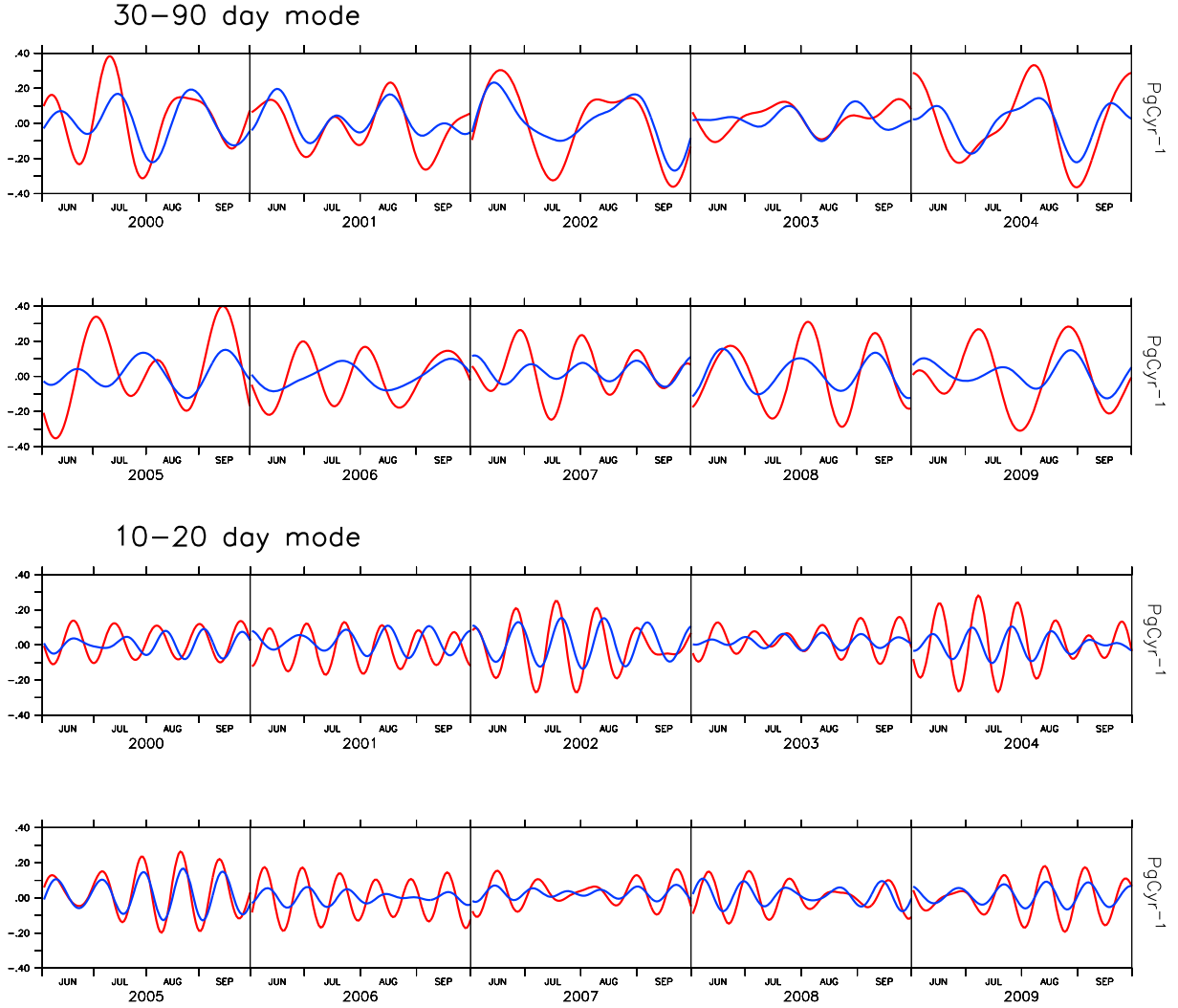


**Figure 5.** The 30–60 day (top) and 10–20 day (bottom) filtered and area-integrated CO<sub>2</sub> flux anomalies from central India (over an area of 72°E–83°E; 18°N–28°N) for the summer monsoon months. Filtering is applied for each year separately. Units are in PgCyr<sup>-1</sup>. The blue (red) line represents CT (VISIT) data. The VISIT data are multiplied by a scale factor of 2 in order to fit its y axis comparable with CT data.

used to simulate VISIT were taken from the Japanese 25 year reanalysis (JRA-25)/JMA Climate Data Assimilation System (JCDAS) [Onogi *et al.*, 2007]. Precipitation bias in JRA-25/JCDAS was corrected prior to the model simulations based on the methods of Saito *et al.* [2011]. In VISIT, NPP is estimated as GPP – RE, where GPP is estimated from the following equation:

$$\text{GPP} = \int_0^{\text{LAI}} \frac{P_{\text{max}} \text{LUE PPFD}}{P_{\text{max}} + \text{LUE PPFD}} d\text{LAI} \quad (6)$$

[19]  $P_{\text{max}}$  is a seasonally varying function of ground temperature, intercellular CO<sub>2</sub> concentration, and moisture. LAI is the leaf area index, LUE is the light use efficiency, and PPFD is the photosynthetic photon flux density within the canopy. The respiration fluxes assume two forms, Autotrophic (AE) and Heterotrophic (HR) respiration. The AE is subdivided into growth (AG) and maintenance (AR) respiration. These are functions of ground temperature,

specific maintenance respiration rate, and  $Q_{10}$ . The maintenance respiration assumes the following form:

$$\text{AR} = r_{\text{mx}} \exp \left[ \frac{\ln Q_{10}}{10} (T_g - 15) \right] M_x \quad (7)$$

[20] The growth respiration is given as a function of carbon translocation rate and specific growth respiration. The heterotrophic respirations are subdivided into humus and litter groups, both of them varying with soil temperature at 10 cm and 2 m, respectively, in addition to their soil moisture-dependent variability. The VISIT NEE data available at daily time step from 2000 to 2009 are used in this study. The spatial resolution is 1° × 1° in the horizontal.

[21] In addition to the conventional prognostic modeling in VISIT, 13 of the model parameters are optimized using Bayesian inversion methods (Saito M., A. Ito and S. Maksyutov, Synthesis modeling of atmospheric CO<sub>2</sub> variability and terrestrial biomass with inversion scheme,

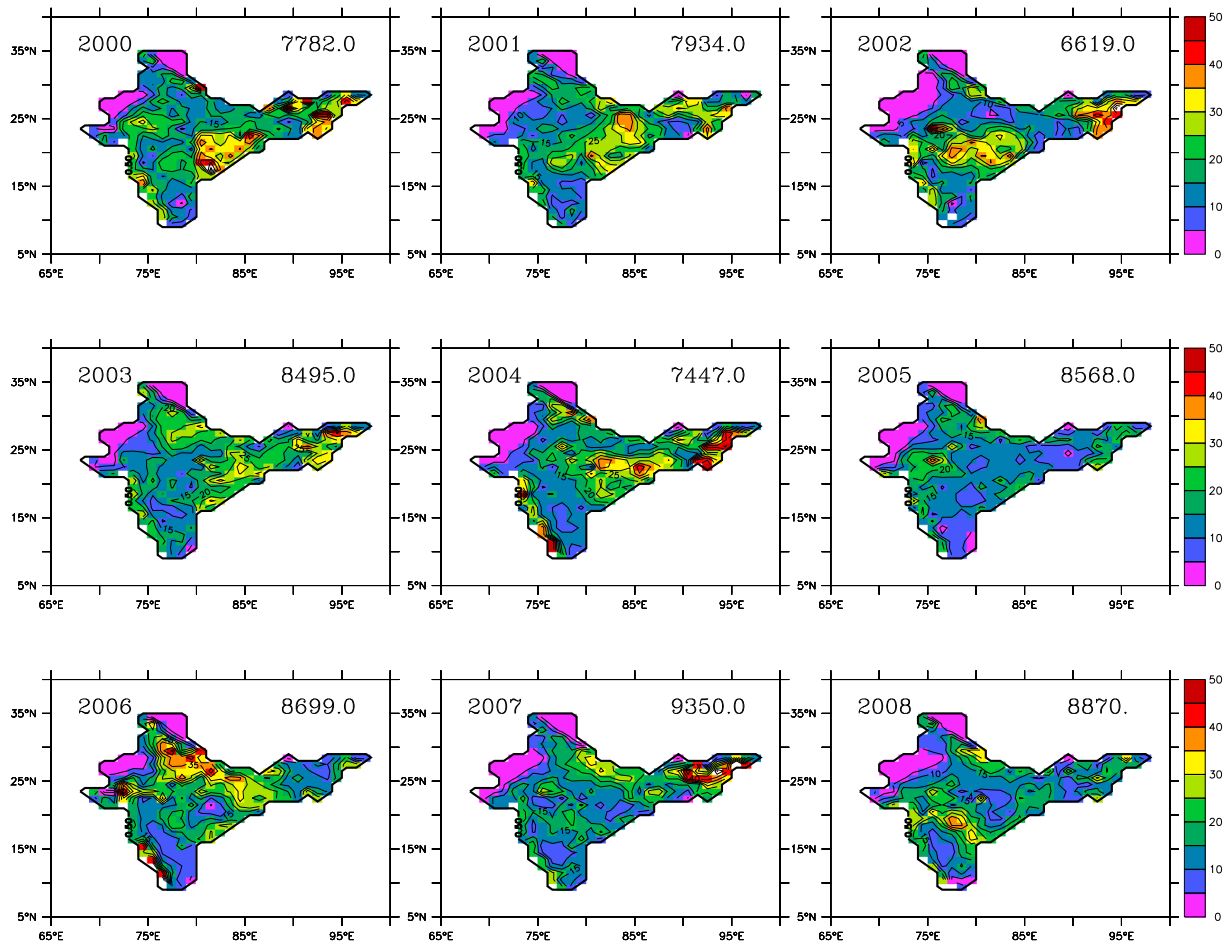


**Figure 6.** Spatial pattern of CO<sub>2</sub> sources for those days with 1 standard deviation or above amplitudes in 30–60 day filtered CO<sub>2</sub> flux anomalies.

manuscript submitted to *Global Biogeochemical Cycle*, 2012, hereinafter SIM, 2013). These 13 of the model parameters are optimized in the following way. The VISIT-simulated NEE (priors) is used to run an atmospheric transport model to convert fluxes into equivalent atmospheric CO<sub>2</sub> mole fractions. The difference between the observed atmospheric CO<sub>2</sub> mole fractions and that of the model simulations is minimized with the Bayesian inversion where the control variables are set as 13 model parameters for 15 biomes in the VISIT. In a similar way, the same model parameters are also optimized based on data for annual mean above-ground biomass and NPP [Maksyutov *et al.*, 2012]. Each of the 13 parameters is optimized separately for the 15 biomes.

[22] Among the 13 model parameters that are optimized,  $Q_{10}$  is one and its prior global mean value (for 15 biomes) is set as 2.0. Via the optimization, the  $Q_{10}$  is found to vary from 1.68 to 2.32 according to biome type. The Crop Land (CL)  $Q_{10}$  has been optimized to 1.85. The CL is one of the dominant types of ecosystem found over the Indian land mass. This value is somewhat higher than the recent estimates of global  $Q_{10}$  ( $1.4 \pm 0.1$ ) irrespective of the annual mean temperature [Mahecha *et al.*, 2010]. On the other hand, Atkin *et al.* [2008] suggest that the acclimation of RE to varying temperatures must be represented in global climate-vegetation models by accounting for a correspondingly varying  $Q_{10}$  especially in high-temperature biomes (such as the ones that span India).

[23] Here we summarize the key differences between CASA used in CT and the VISIT model processes. CASA was run with ECMWF re-analysis on monthly time scales. The sub-monthly (hourly and synoptic) variability was introduced by simple relations (equations (2)–(5)). The NDVI data used are from AVHRR. The VISIT model used JRA-25 meteorology, 13 model parameters are optimized based on Bayesian inversion with CO<sub>2</sub> atmospheric data, above-ground biomass data, and NPP data. The NDVI used is from MODIS. The optimized  $Q_{10}$  varied from 1.68 to 2.32 for 15 biomes. The RE is split into two, to account for the fine details of respiration pools (equations (6) and (7)). We highlight these differences in order to show how the different details of biospheric processes were included in these two models and hence to validate the results.

### 2.3. Rainfall Data

[24] For analysis purpose, we made use of daily rainfall data taken from APHRODITES water resources [Yatagai, *et al.*, 2009]. This data set is created primarily from data obtained from rain gauge networks. These data are available at  $0.25^\circ \times 0.25^\circ$  resolution at daily time scale. The 2 m temperature data derived from ERA-interim re-analysis for the period of 2000 to 2009 are also used in this study [Dee *et al.*, 2011, Simmons *et al.*, 2007].

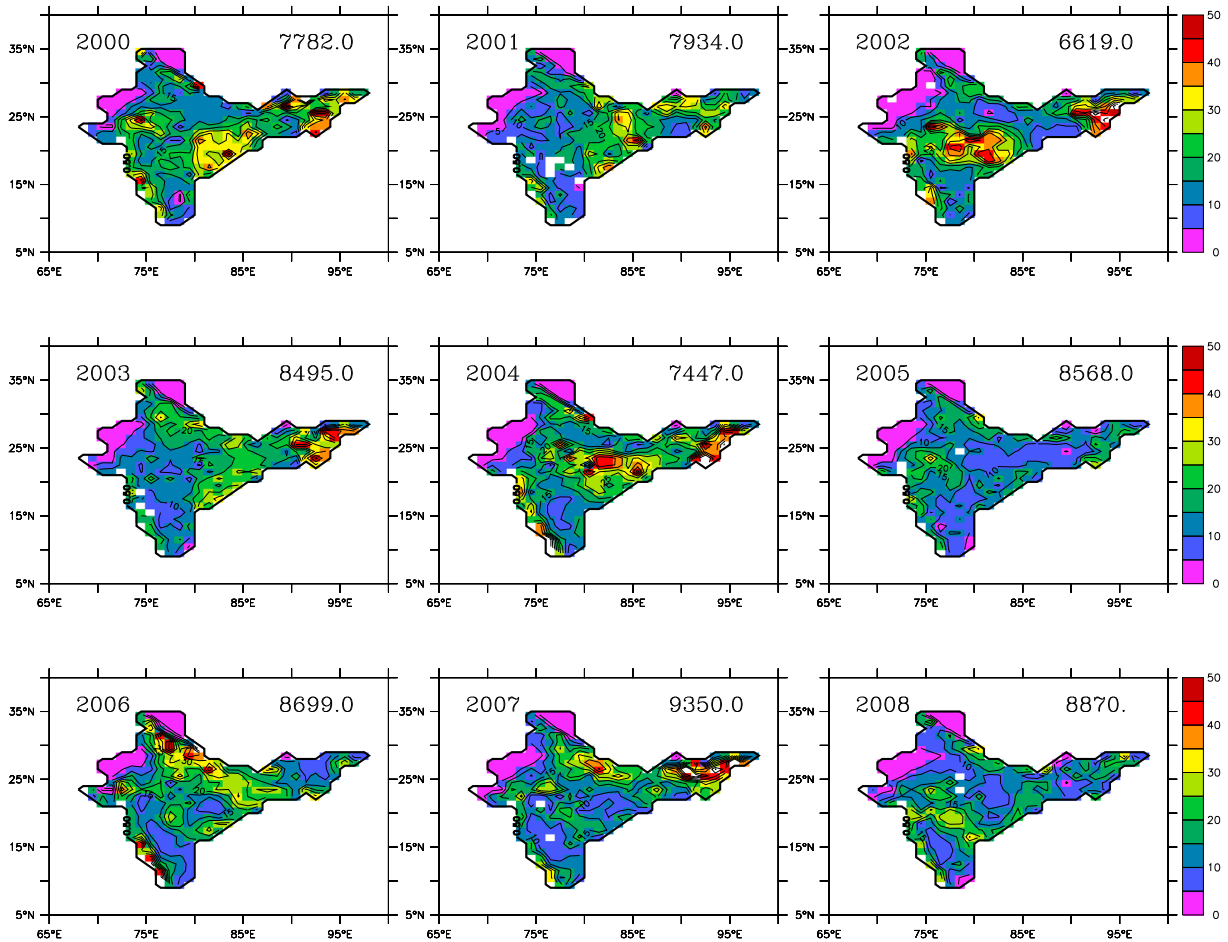


**Figure 7.** Same as Figure 6 but for those days with  $-1$  standard deviation or below CO<sub>2</sub> sinks.

#### 2.4. Power Spectrum Analysis

[25] In order to depict the ISOs in the terrestrial biospheric fluxes over the Indian region, we carried out a power spectrum analysis. For each year, the daily CO<sub>2</sub> fluxes from June to September (122 days) at each grid point were separated into Fourier components and the powers with largest amplitudes were found. The daily CO<sub>2</sub> flux anomalies were obtained before applying the Fourier filtering in order to remove the red noise in the resulting spectra. Here, the anomalies were found by removing the first three harmonics (annual, semi-annual, and quadra-annual cycles) of CO<sub>2</sub> fluxes from each grid point for each year.

### 3. Results

[26] In Figure 1, we show the vegetation cover over India classified into 20 types according to the Global Land Cover Characterization (GLCC) data sets as derived from the 1 km Advanced Very High Resolution Radiometer (AVHRR) data spanning April 1992 to March 1993 (more information regarding GLCC data sets can be found at <http://edcdaac.usgs.gov/glcc/glcc.html>). Throughout central India, the crop/mixed farming dominates the land cover type. The vegetation yield of the region thus heavily depends on the net summer monsoon rainfall [Gadgil and Rupa Kumar, 2006; Preethi and Revadekar, 2012]. The second

largest vegetation type in the central India is forest cover. The irrigated crop is largely distributed over the southeastern peninsular region where the summer monsoon rainfall is relatively low. The figure also shows the climatological mean normalized difference vegetation index (NDVI) during 1982–2000. Figure 1b shows the annual mean NDVI over the Indian subcontinent and Figure 1c shows its seasonal cycle. The country's overall vegetation growth increases from June and peaks in September and October.

#### 3.1. Seasonal Cycle of NEE Over India

[27] Figure 2 shows the monthly means of the climatological land-to-atmosphere CO<sub>2</sub> fluxes for the four summer months during monsoon rainfall, derived from CT between 2000 and 2009 (Figure 2a). In this climatology, the anomalously dry years (i.e., 2002 and 2004) were excluded. The fluxes are positive (from land to atmosphere) during June and July, generally throughout India with a peak amplitude of  $50 \text{ mol m}^{-2} \text{ yr}^{-1}$ . The monsoon rainfall over India typically starts in June and matures in July [Goswami, 2005]. A typical feature of CO<sub>2</sub> fluxes during June and July is that the terrestrial ecosystem NPP does not exceed respiration resulting in a positive NEE during this period (interpreted from the positive values of CO<sub>2</sub> fluxes in Figures 2a and 2b). On the other hand, from early August to September, the terrestrial biospheric fluxes over India dramatically shift to a sink over almost the entire

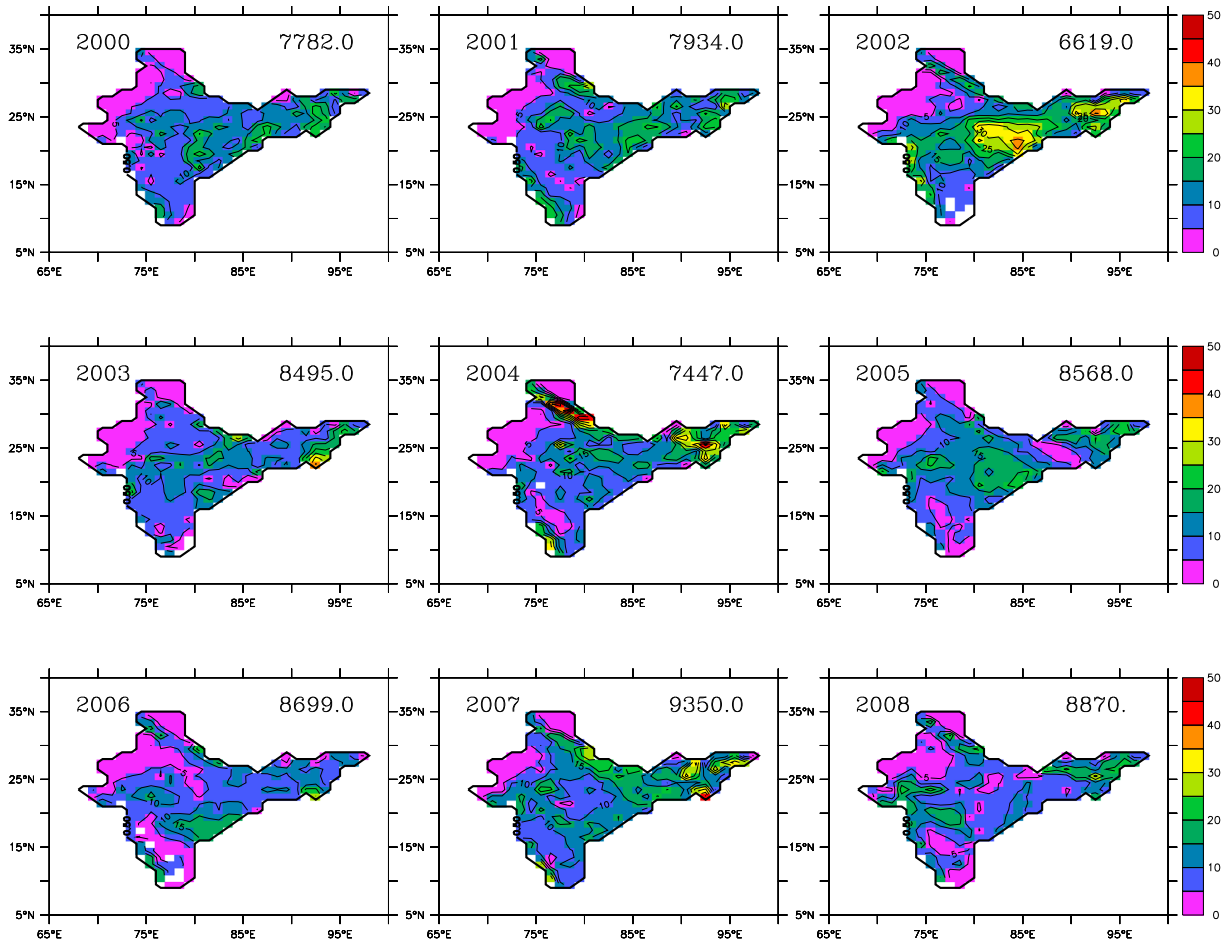


**Figure 8.** Same as Figure 6 but for 10–20 day filtered CO<sub>2</sub> flux anomalies.

continent with peak amplitude of  $30 \text{ mol m}^{-2} \text{ yr}^{-1}$  (Figures 2c and 2d). The largest sink is found over central India during September.

[28] Figure 2e shows the area-integrated terrestrial biospheric CO<sub>2</sub> fluxes from Indian subcontinent during each month from 2000 to 2009. The shade enveloping the line is the daily standard deviation during each month calculated with respect to the corresponding monthly climatological mean. The seasonal cycle of area-integrated CO<sub>2</sub> flux shows a peak emission during June–July, changes to a steep reduction in source, and then turns to a strong sink during late September. The daily standard deviation shows that the strongest high-frequency variances (i.e., sub-monthly variability) occur during June and July when the CO<sub>2</sub> flux is strongly positive and during September when the CO<sub>2</sub> flux is strongly negative.

[29] The seasonal cycle of NEE from CT data was compared with that derived from the atmospheric inversion study of *Niwa et al.* [2012] for the period between 2006 and 2008 (Figure 2e, red line, amplitude is scaled by half). In this inversion, the aircraft-observed atmospheric CO<sub>2</sub> data collected by Japanese airliner were also used in addition to the CO<sub>2</sub> data used in CT inversion. The inclusion of aircraft-observed CO<sub>2</sub> data into the inversion has reduced the posterior error of NEE from the Indian region by 30–40% [*Niwa et al.*, 2012]. The seasonal cycle of NEE from CT and *Niwa et al.* [2012] compares fairly well although minor phase shift is visible.

[30] Figures 3a–3e show the corresponding spatial and seasonal cycle of NEE over India obtained from the VISIT optimized data. The spatial pattern of NEE from the VISIT data from June to September shows similar features as in CT. The June–July area-wide sources and August–September area-wide sinks are nearly identical between the two data sets compared here. However, VISIT shows high values of terrestrial sinks in the foothills of Himalayas and the northern and northeastern parts of India. These values have been masked, and an area integral is shown in Figure 3e. The seasonal cycle and sub-monthly standard deviations are comparable in the two data sets. However, VISIT shows a weaker seasonal cycle and a stronger sub-monthly variability. The strong emission during March to May clearly seen in CT is barely visible in VISIT. The delicate balance of carbon flows between terrestrial ecosystem and atmosphere is rather complex, and the two models represent these complex biospheric processes in their own way. The VISIT NEE shown here is a reasonable reproduction of the same reported in *Niwa et al.* [2012].

### 3.2. ISOs of CO<sub>2</sub> Fluxes Over the Indian Subcontinent

[31] Figure 4 shows the periods (in days) at which the spectral power is maximum at each grid point and is shown separately for individual years (see section 2.4 for methods of power spectrum analysis). Majority of the regional CO<sub>2</sub> fluxes over India display a clear intraseasonal oscillation

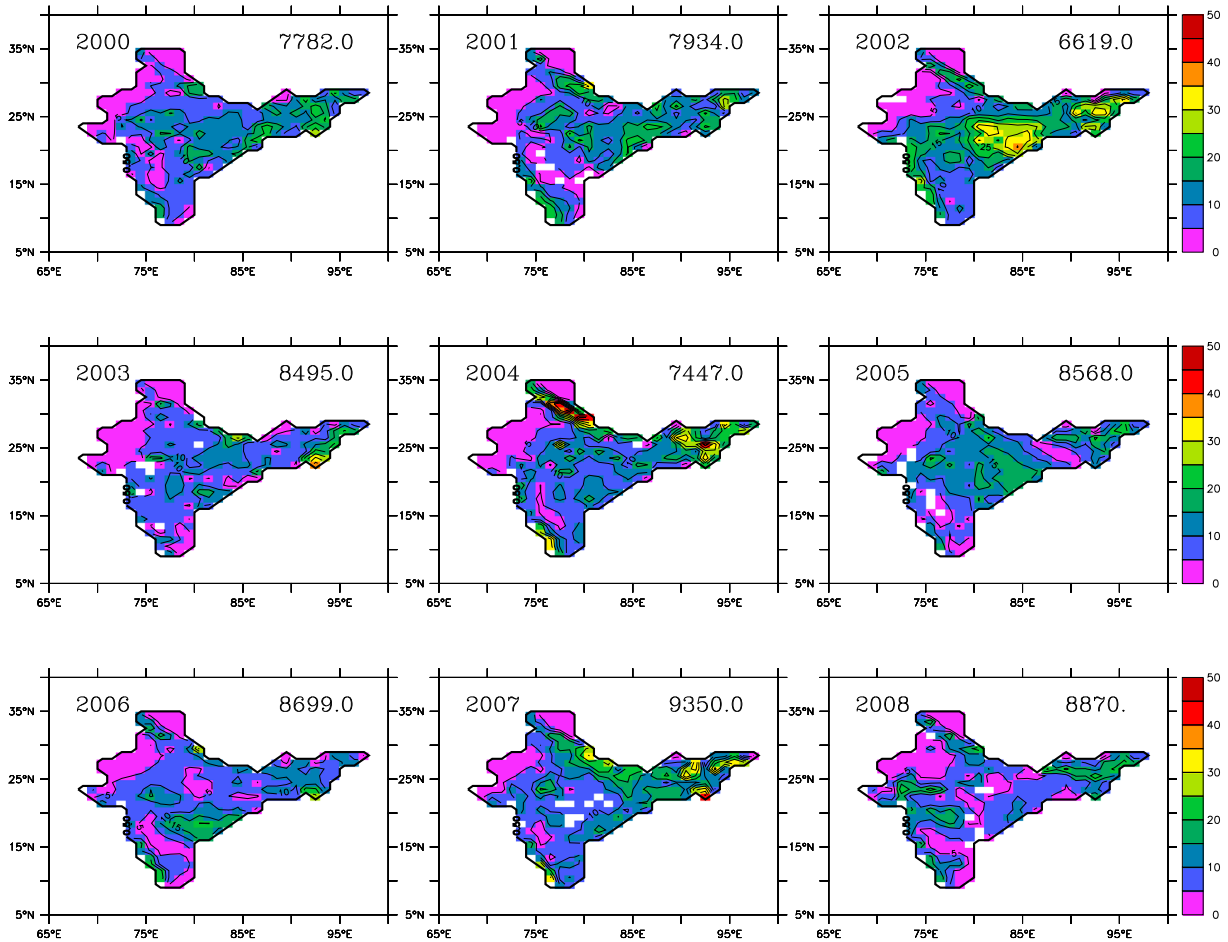


**Figure 9.** Same as Figure 7 but for 10–20 day filtered CO<sub>2</sub> flux anomalies.

with a period of  $\sim 60$  days. Notably, this cycle of variability is spatially dominant especially when the monsoon rainfall is relatively weak or when it is a drought year. For a comparison of monsoon rainfall strength in terms of rainfall, Figure 4 is provided with the annual mean monsoon rainfall received during each year. For instance, the year 2002 was a typical drought year for the monsoon rainfall [Valsala and Ikeda, 2005] and was dominated by a 60 day or longer periodicity in the ISO of the CO<sub>2</sub> fluxes. On the contrary, year 2007 had an above-normal monsoon rainfall and was characterized by relatively higher frequency variability in the CO<sub>2</sub> fluxes and with more heterogeneous structure in space. The corresponding analysis using the VISIT NEE fluxes also showed similar results (figure not shown). The VISIT NEE flux intraseasonal variability is compared in the following paragraphs.

[32] The most general feature visible in Figure 4 is that the regional CO<sub>2</sub> fluxes possess a clear ISO signature with the period ranging from 10 to 60 days. Based on this information, we further applied a harmonic filter to extract the variability between two distinct bands, namely a 10–20 day band and 30–60 day band. The following part of this section describes the variability of CO<sub>2</sub> fluxes in these two bands.

[33] Figure 5 shows the intraseasonally filtered CO<sub>2</sub> flux anomalies from the central Indian region (spanning 72°E–83°E and 18°N–28°N) for each year from 2000 to 2009 for the summer monsoon season. The choice of this region was made based on previous studies [Rajeevan

*et al.*, 2010; Pillai and Sahai, 2012] in which this region was found to represent the essence of the ISOs of monsoon rainfall. In Figure 1, we noted that this box comprises largely of vegetation consisting of crops and mixed farming and to some extent also the forest cover. The anomalies are filtered for two distinct bands as stated above. Hereinafter, the positive (negative) anomalies mean a source (sink) of CO<sub>2</sub> at ISO time scales only, while the mean value over the whole month can be either a net source or sink (see Figures 2e and 3e for the seasonal cycle of net NEE over India). The CT data show that the peak-to-peak amplitude of CO<sub>2</sub> flux anomalies in the 30–60 day mode is nearly 0.6 Pg C yr<sup>-1</sup> which is nearly 30% of the peak-to-peak amplitudes of CO<sub>2</sub> fluxes between June and September. It is worth noting that the 30–60 day mode variability of CO<sub>2</sub> fluxes has higher amplitudes than 10–20 day modes (Figure 5). Therefore, the central India terrestrial biospheric fluxes may be generally dominated by a slowly varying 30–60 day mode.

[34] A similar analysis carried out with the VISIT data showed that the ISO variability is weaker in VISIT compared to that derived from CT data. In Figure 5, the VISIT anomalies are scaled by a factor of 2, to facilitate comparison with a common  $y$  axis. Therefore, the VISIT ISOs suggest only 50% of the CT amplitude in intraseasonal variability. However, we note that the daily standard deviation with respect to each month in Figure 3 shows that VISIT has larger variability in sub-monthly scales, although its ISOs are weaker.

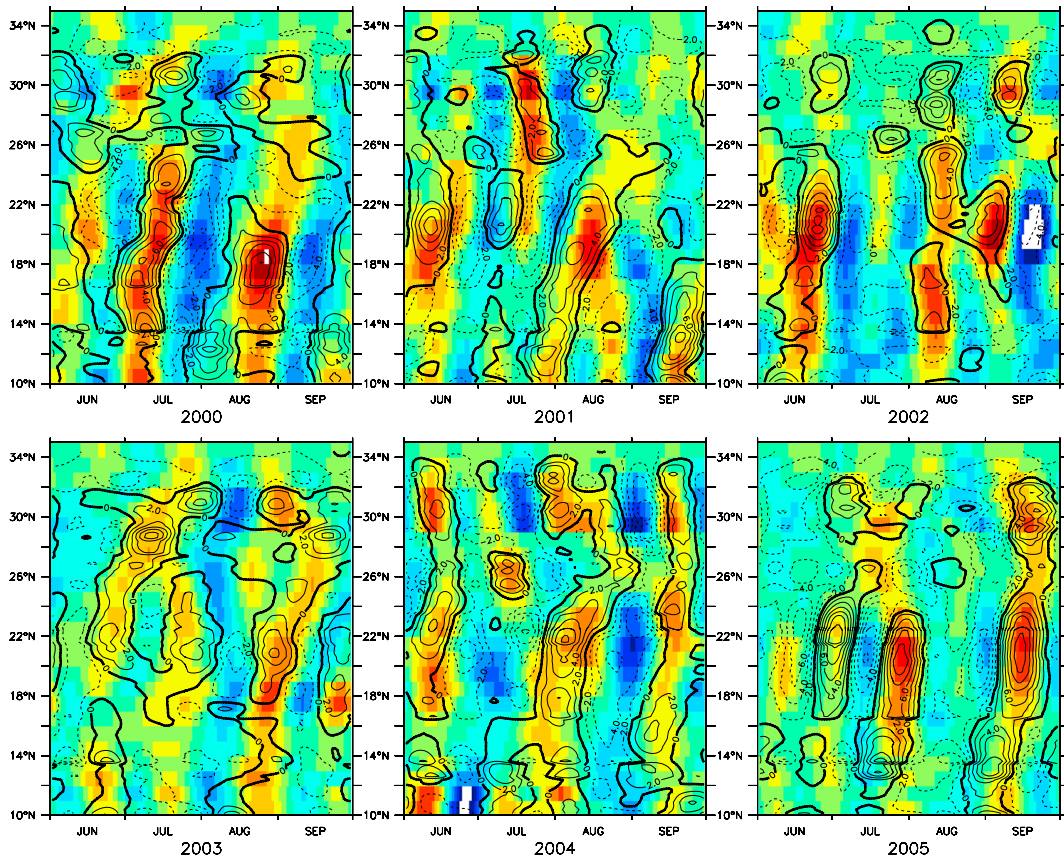


**Figure 10.** The 30–60 day filtered and zonally integrated (over 65°E–95°E) CO<sub>2</sub> fluxes (shades) and daily rainfall (contours).

[35] A striking feature that emerges from Figure 5 is that the intraseasonally filtered anomalies of terrestrial CO<sub>2</sub> fluxes over central India show consistent variability between CT and VISIT data sets. This is comforting as far as the process understanding is concerned at least in terms of two distinctly different models capturing a nearly identical terrestrial biosphere response at intraseasonal time scales and thus should provide good guidance for gathering necessary data to confirm the results further from observations. Both these models derive their terrestrial NEE with varying complexities in the ecosystem processes. For example, the CT uses its prior NEE on CASA simulated fluxes, whereas the VISIT is an entirely different ecosystem model (see section 2 for differentiating the two model processes). Moreover, the meteorology used to drive these models comes from two different re-analysis products. Thus, even with different approach and forcing data, the models yield similar results. The agreement between the models is visible not only in the individual year’s ISOs but also in their year-to-year variability. Therefore, we can confidently assert that the terrestrial ecosystem over Indian region shows coherent patterns of variability with summer monsoon variability.

[36] Figures 6 and 7 show the composites of net source and sink of terrestrial biospheric CO<sub>2</sub> fluxes over India in the 30–60 day band for each year from the CT data. Similar results were obtained with the VISIT fluxes as well, although for brevity, we focus our discussion on only the CT data. The composite is produced by averaging those events during which the CO<sub>2</sub> source (sink) is above

positive (below negative) one standard deviation in the filtered time series at each grid point. Figure 6 shows that the intraseasonal “respiration” (i.e., biospheric CO<sub>2</sub> emissions) of terrestrial biosphere over the Indian region has a nearly homogeneous pattern from year to year although the spatial heterogeneity is quite noticeable. The maximum amplitude is found over central India. The leeward side of the Western Ghats (a mountain range along the western peninsular India), however, has relatively small amplitude of respiration (in terms of CO<sub>2</sub> sources). Figure 7 shows the corresponding CO<sub>2</sub> sinks.

[37] In Figures 8 and 9, we show a similar calculation but for the anomalies filtered for the 10–20 day band. In this case, the figure depicts high frequency variability of CO<sub>2</sub> fluxes over the Indian continent. A noticeable difference of CO<sub>2</sub> variability in the 10–20 day band from that of the 30–60 day mode is that the former is relatively weak in amplitude and spatially more homogeneous. This point is also reflected in Figure 5 where we examined the variability of the spatially integrated CO<sub>2</sub> fluxes over central India. The important message from Figures 8 and 9 is that the high-frequency variability of CO<sub>2</sub> fluxes over India is weaker and that this variability may not make a significant contribution to the net CO<sub>2</sub> fluxes.

### 3.3. Coherence of ISOs of CO<sub>2</sub>, Rainfall, and Temperature

[38] The NPP of terrestrial biosphere should respond to the variability in air-temperature, PAR, and rainfall, and all of these are also a part of the monsoon ISOs. Therefore, in this

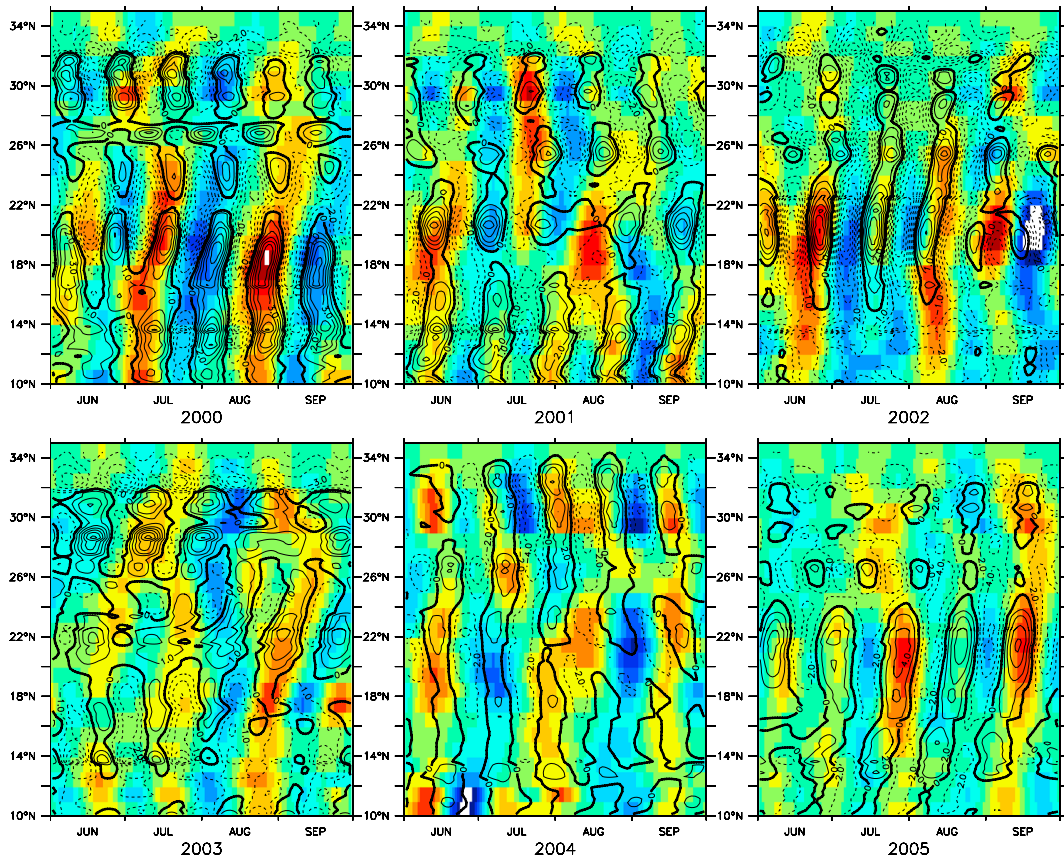


**Figure 11.** Same as Figure 10 but for 10–20 day mode.

section we look for coherent structures of oscillations between CO<sub>2</sub> and other physical parameters that participate in the summer ISOs. In order to understand the co-variability of the ISOs of CO<sub>2</sub> flux and monsoon rainfall, we calculated the 30–60 day and 10–20 day band-pass-filtered monsoon rainfall anomalies from the APHRODITE rainfall data. As the simplest illustration of coherency between the ISOs of CO<sub>2</sub> flux and rainfall, we show the zonally averaged precipitation anomalies (filtered) of monsoon rainfall over India together with the zonally integrated CO<sub>2</sub> fluxes (filtered) over the same region.

[39] Figure 10 shows the 30–60 day band-pass-filtered anomalies from the CT data. We find that they correlate in most of the years examined here. Positive anomalies of CO<sub>2</sub> fluxes appear to be correlated with positive rainfall anomalies. On the contrary, negative anomalies of CO<sub>2</sub> fluxes appear to be correlated with negative anomalies in rainfall. The message we deliver from this analysis is that respiration exceeds NPP when rainfall anomalies are positive at ISO time scales, possibly indicating the direct effect of the deficiency of PAR when organized clouds shade NPP during the active spells of rainfall. Moreover, the heterotrophic respiration can surge during sudden rain events and can contribute to positive NEE [Xu *et al.*, 2004]. On contrary, NPP exceeds respiration and results in a net CO<sub>2</sub> sink on ISO time scale when rainfall anomalies are negative (i.e., during break spells) and clear sky conditions lead to increased PAR on intraseasonal scales. While this is rather counter-intuitive, it should be noted that even the most severe droughts typically result in overall rainfall

deficiency of  $\sim 20\%$  [Goswami, 2005] and thus may not affect the terrestrial biosphere response severely in terms of CO<sub>2</sub>. Therefore, the Indian terrestrial biospheric fluxes undergo a tandem oscillation at the ISO time scale in correspondence with variability in rainfall. The amplitude of this oscillation is about 25% of the mean value during monsoon rainfall.

[40] In order to investigate whether this coherency is solely at the 30–60 day band, we also examined the co-variability of CO<sub>2</sub> flux and monsoon rainfall anomalies in the 10–20 day band. Figure 11 shows that this coherency is equally strong in the high-frequency mode as well. Therefore, we hypothesize that such immediate and approximately in-phase response of CO<sub>2</sub> fluxes to the monsoon rainfall may be directly related to the PAR shielding by the organized clouds during active and break spells of rainfall (see also equations (2)–(5)). This is reminiscent of the marine ecosystem organization by the MJOs as observed in the ocean color data [Waliser *et al.*, 2005; Jin *et al.*, 2012]. An examination of surface shortwave radiation to infer the PAR variability on ISO scale follows to explore the mechanistic links.

[41] In addition to its sensitivity to radiation, the terrestrial biospheric fluxes are also tied to the variability in the ambient air temperature. Therefore, we examined the air-temperature anomalies filtered at these two distinct bands (i.e., 30–60 days and 10–20 days) which are the intrinsic properties of summer monsoon ISOs. In this temperature-CO<sub>2</sub> analysis (figure not shown), we found apparent lags between air-temperature ISOs and CO<sub>2</sub> flux ISOs. In order to clearly establish the lead-lag relations of ISOs of CO<sub>2</sub>, monsoon rainfall, and

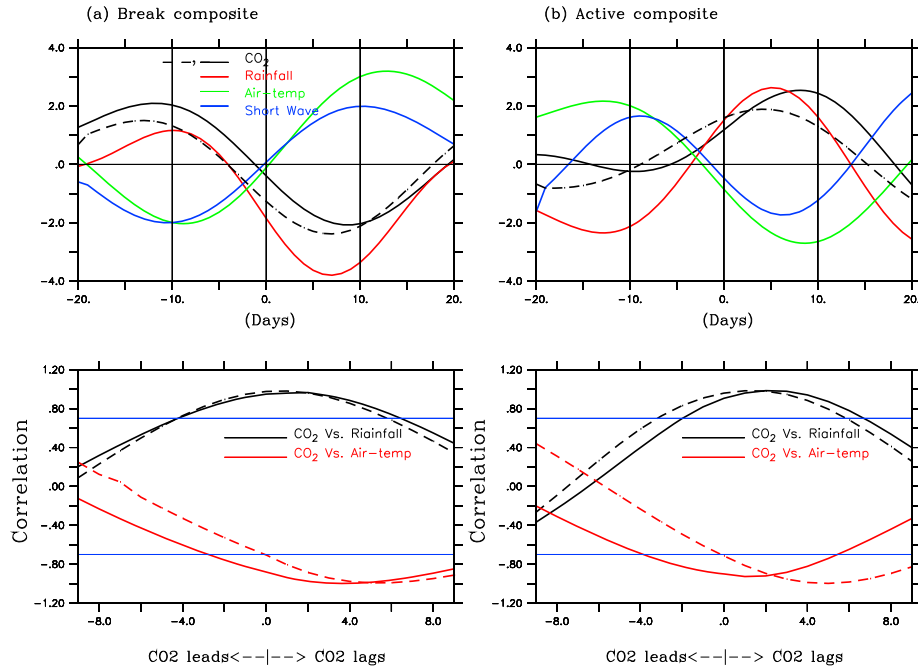


**Figure 12.** Break and active phase composites of rainfall with CO<sub>2</sub>, 2 m air-temperature, and surface shortwave radiation anomalies at corresponding periods from filtered anomalies at a 30–60 day band. Break and active phases are identified by applying a similar method as *Krishnan et al.* [2000] and *Pillai and Sahai*, 2012]. Day 0 represents a starting of break or active phase. All such events from each year are averaged to produce the composite. CT (VISIT) data are represented by full (dash) lines. The VISIT data are multiplied by a scale factor of 2 in top panels in order to fit its  $y$  axis comparable with CT data. The units of CO<sub>2</sub> fluxes are in  $\times 10^5 \text{ mol s}^{-1}$ . Unit of rainfall is in millimeters. Unit of air-temperature is in  $\times 10^{-1}^\circ\text{C}$ . Unit of shortwave is in  $\times 10 \text{ Wm}^{-2}$ .

air-temperature, we adapted a composite analysis of “break” and “active” phases of monsoon rainfall as follows.

[42] Two distinct phases of ISO are identified—(a) the break phase and (b) the active phase. The “break” phase here is when the ISOs of the monsoon rainfall anomalies are negative and correspond to positive CO<sub>2</sub> anomalies and air-temperature anomalies with a lag to monsoon rainfall. We used the “break” phases of monsoon rainfall as a bench mark to study the distinct positive anomalies of CO<sub>2</sub> on ISO time scales because our goal is to establish the ISOs of CO<sub>2</sub> and their relation to corresponding variability of monsoon rainfall. The break phases of monsoon rainfall are identified as in *Krishnan et al.* [2000]. The box-averaged outgoing longwave radiation (OLR) over central India [see *Rajeevan et al.*, 2010] is used as an identifier of the break spell of the rainfall. The CO<sub>2</sub> flux anomalies for 20 days before and after the break are identified for each year and all such events are averaged to find the break composite. The same is repeated with “active” phases as well. The monsoon rainfall and the 2 m air-temperature as well as surface shortwave radiations were also composited in a similar manner.

[43] Figure 12 shows a composite of CO<sub>2</sub> flux (both from CT and VISIT data), rainfall, air-temperature, and surface shortwave radiation (proxy for PAR) anomalies during the break and active phases of summer monsoon averaged over the central Indian box. As expected, the CO<sub>2</sub> flux and rainfall anomalies during both the break and active phases have identical evolution. This is equally visible in both CT

(black solid line) and VISIT (black dash line). However, a closer examination reveals that the CO<sub>2</sub> flux lags the rainfall by 2–3 days in the case of CT. This lag is slightly shorter (more or less at 1 day) in the case of VISIT. In order to clarify the lead-lag relationship between the three parameters examined here, we also show a lead-lag correlation between them in the bottom row of Figure 12. In the case of CT data, the correlation between CO<sub>2</sub> and rainfall peaks at 2–3 days of lag for both break and active phases. Therefore, the response time of CO<sub>2</sub> to rainfall events at ISO time scale is rather fast (within a matter of 2–3 days), and this property is visible both in break and active phases of monsoon rainfall. This may partially point to the lead-lag changes in PAR, NPP, and both autotrophic and heterotrophic respirations. This lag has been, however, reduced to 1–2 days in the case of VISIT data. Such subtle changes between the data are understandable because of the complexities in the model processes which couple various physical parameters and plant phenology in a complex manner. Overall, the agreement between both the data in the ISO phase evolutions with air-temperature is rather remarkable and may be indicative of the robustness of the relation between CO<sub>2</sub> and other parameters on the intraseasonal time scales that are shown here.

[44] The air-temperature has more than 120° of phase lag with the CO<sub>2</sub> flux anomalies at ISO time scales during the break phase. The correlation between CO<sub>2</sub> and air-temperature peaks at a lag of 4–5 days (i.e., CO<sub>2</sub> lags air-temperature) during the break phase whereas during the active phase this lag is down at 2–3 days. This is a remarkable change

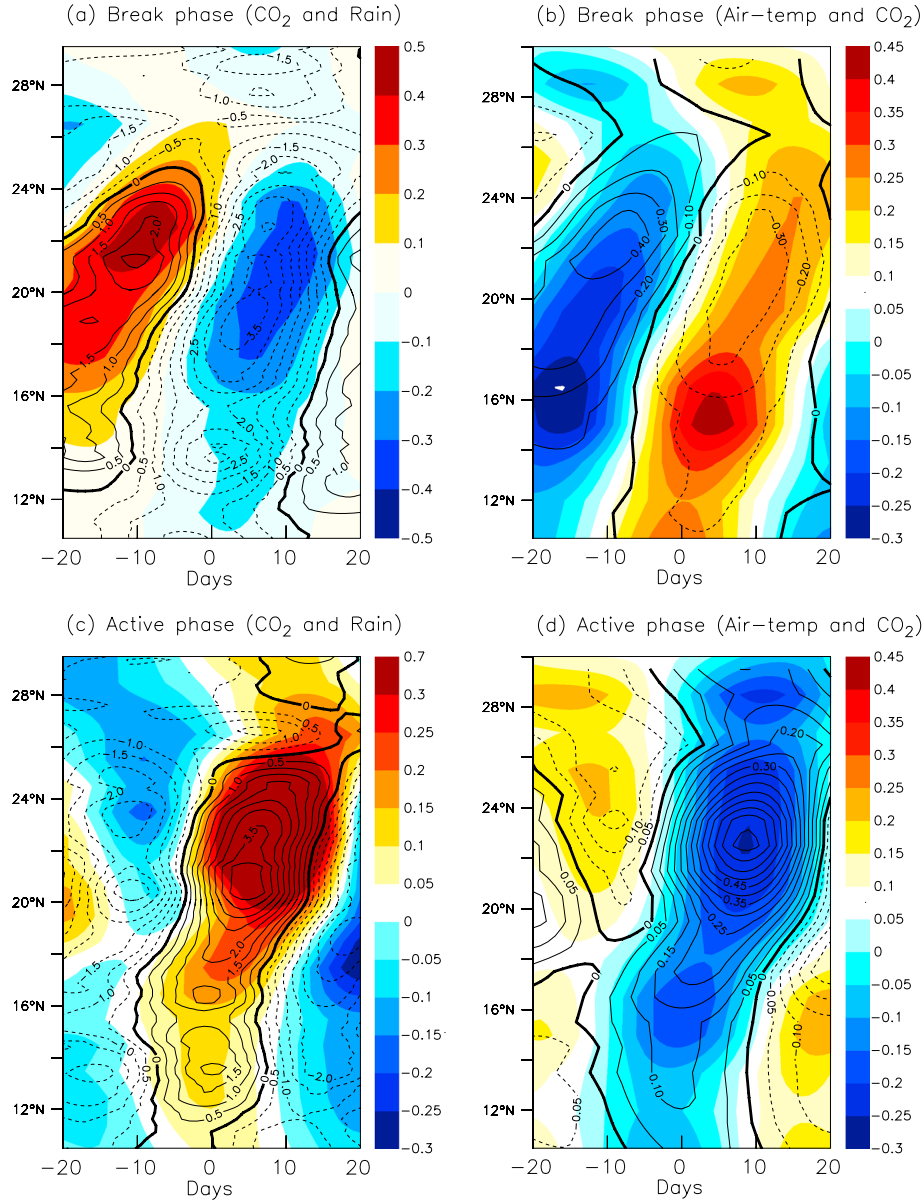


**Figure 13.** Same as Figure 11 but shown as a space-time section of break and active phases as averaged zonally (integrated in case of CO<sub>2</sub>) over India. In the left column, shades (contours) represent CO<sub>2</sub> flux (rainfall). In the right column, shades (contours) represent 2 m air-temperature (CO<sub>2</sub> flux).

between active and break phases in response to time scales of ISOs of CO<sub>2</sub> and air-temperature. *Atkin et al.* [2000] reported that a similar RE acclimation to short-term temperature changes occurred on the order of 1–3 days. The PAR variability is also in phase with air-temperature and therefore the CO<sub>2</sub> flux varies inversely to PAR (see the shortwave radiation variability in the Figure 12), i.e., when PAR is positive the biosphere is a sink of CO<sub>2</sub> and vice versa on ISO time scales. This strengthens our hypothesis that direct shading by organized clouds during monsoon rainfall can cause CO<sub>2</sub> flux variability in the ISO band.

[45] We should note that the differences in the results between the two data sets are more obvious in the active phase than in the break phase. The correlation of CO<sub>2</sub> with rainfall has a nearly 2–3 day lag in CT, whereas it is almost in-phase in the case of VISIT. The correlation

with temperature variability in CT is lagged by nearly 2–3 days, but longer (4–5 days) in the case of VISIT. Again such subtle changes might be expected when complexities in the model vary, pointing again to the need for more observations.

[46] The phase differences between the 2 m air-temperature and rainfall anomalies are explained by a mechanistic link with the ISOs of monsoon rainfall [*Krishnamurthy and Shukla*, 2000; *Goswami*, 2005]. The air-temperature is colder prior to the break (–20 to 0 days in Figure 12a) because of the cloud cover and rainfall. By the arrival of a break in rainfall, the air-temperature rises fairly rapidly because the cloud free conditions allow more shortwave to reach the surface. Photosynthesis and respiration increase with air-temperature. At optimal conditions of temperature range, photosynthesis overwhelms respiration and causes a

net sink of CO<sub>2</sub> during the break phase. The situation is opposite during an active phase, i.e., prior to the active phase, the NEE is a net (weak) sink and transitions to a source fairly rapidly once the rainfall commences. This again indicates that the cloud cover and the resulting reduction in radiation for plant growth are the key for biospheric response. It is worth noting that during the  $-20$  to  $0$  day period of an active phase, NPP is maximized and the CO<sub>2</sub> sink is nearly zero. This may be a combined effect of moisture loss during the break phase and an increase in respiration. In most of the plants, respiration increases quite linearly with air-temperature whereas photosynthesis saturates above an optimal temperature [Goudriaan *et al.*, 2001].

[47] It is worth examining the lead-lag relation between CO<sub>2</sub> and rainfall further. The CO<sub>2</sub>-rainfall relationship can be attributed to radiation changes with respect to the changes in cloud cover during active and break rainfall events. In this case, an immediate response of CO<sub>2</sub> to rainfall variability at zero-lag is expected. However, the air-temperature (which itself is lagged with respect to the rainfall on ISO time scales) may influence NPP and RE. We examined the possibility of whether the effects of temperature on NEE and RE can lead to a lagged relation between CO<sub>2</sub> and rainfall. We employed a partial correlation analysis in order to remove the variability of temperature on CO<sub>2</sub> fluxes. Partial correlation selectively removes the effect of one parameter over the other two when the three of them are mutually correlated. We found that by the “removal” of temperature effects, the correlation between CO<sub>2</sub> and rainfall at zero-lag improved to a level that it had at 2–3 days of lag in the ordinary correlation. This is the case for CT data. The corresponding shift in correlation in VISIT data is at about 3–4 days of lag. This suggests that the ISO time scale air-temperature variability may have a “grip” on the corresponding CO<sub>2</sub> flux variability and leads to a lagged correlation between CO<sub>2</sub> and rainfall. The mechanism by which the lag between CO<sub>2</sub> and rainfall is induced may be due to temperature effects. This can be quite different in break and active phases because in the latter case, the CO<sub>2</sub>-temperature lag itself is shorter (2–3 days) than in the former (3–4 days; see Figure 12).

[48] The area-averaged phase relationship between CO<sub>2</sub> fluxes, rainfall, and 2 m air-temperature gives the net ISO response of biospheric CO<sub>2</sub> fluxes during both the active and break phases of the monsoon over central India. In Figure 13, we illustrate the time-space evolution of this relationship as zonally integrated CO<sub>2</sub> flux anomalies of the composite active and break phases together with the area-averaged rainfall and temperature anomalies for the CT data. VISIT also yields similar results (figure not shown). As stated in the introduction, ISOs have a northward propagating component especially in the 30–60 day band. This northward migration of ISO can be seen in Figure 13 from 12°N to 30°N. In response to these rainfall and temperature migrations, the CO<sub>2</sub> flux anomalies also display a northward propagation. It is interesting to note that the phase locking of rainfall and CO<sub>2</sub> flux anomalies is apparent throughout the entire latitude range. On the other hand, the 2 m air-temperature shows an out-of-phase relationship with CO<sub>2</sub> flux anomalies (Figure 13). The phase relationship between CO<sub>2</sub>, rainfall, and temperature during break and active phase of ISOs is quite consistent with each other, although some differences are evident. For example, the break phase evolution of the intrinsic oscillation of these parameters shows a clear

northward propagation, whereas the corresponding active phase evolutions are somewhat discontinuous in space. These intricate differences may also be inherent to the mechanisms of northward propagations of summer monsoon ISOs [Goswami and Ajayamohan, 2001; Goswami, 2005].

#### 4. Discussions

[49] A few aspects of the ISOs in terrestrial biospheric CO<sub>2</sub> fluxes over the Indian subcontinent during the monsoon rainfall season are identified in this study. Considering the amplitude of variability at the ISO time scale (25% of the seasonal mean in the case of CT and up to 15% in the case of VISIT), ISOs play a considerable role in the seasonal mean CO<sub>2</sub> flux variability over India. The prime factor for this variability may be associated with the direct shielding of sunlight by organized clouds during the wet phases of ISOs leading to reduced CO<sub>2</sub> sink and vice versa for the dry phases, with both phases including the role played by heterotrophic respirations.

[50] Our analyses bring out an unexpected characteristic of CO<sub>2</sub> fluxes during monsoon onsets and breaks; CO<sub>2</sub> sink is stronger during the break phase and is largely driven by availability of PAR and the cloud effects on surface radiation with a corresponding source in the onset phase where rainfall is associated with reduction in PAR. In addition to this process, the heterotrophic respiration also appears to surge during sudden rain spells which can eventually lead to a net positive NEE over NPP [Xu *et al.*, 2004]. The net seasonal variability, however, is related to the integration of rainfall variability by the terrestrial biosphere where the onset of the rainy season itself initiates the growth phase but respiration dominates during June–July and the subcontinent as a whole is a net source of CO<sub>2</sub>. But as the season progresses, the growth phase reaches its peak and during the latter half of the monsoon season, the region acts as a net sink of CO<sub>2</sub>.

[51] The regions where the coherent structures of CO<sub>2</sub>, rainfall and temperature at ISO time scales are detected are dominated by crop and mixed farms (Figure 1). The study brings out an interesting point that the break (active) phases are generally associated with higher (lower) NPP than a combination of autotrophic and heterotrophic respiration. A counterintuitive result is that high NPP during extended break periods does not translate into high crop yields. A drought monsoon year directly relates to a poor crop yield for the country as a whole [Parthasarathy *et al.*, 1988; Preethi and Revadekar, 2012]. This is generally because the water stress over the crop yields during drought years is below the threshold level of relatively extractable water [Ciais *et al.*, 2005]. The crop yield and photosynthetic rate are generally poorly correlated [Long *et al.*, 2006a, 2006b]. Increased photosynthetic rate does not imply a high crop yield because there are other factors such as efficiencies of light capture and of the conversion of the intercepted light into biomass and the proportion of biomass partitioned into grain, etc., that determine the net crop yield during a season. The variability of the net crop yield differs among different genotypes of a crop species and also depending on the net availability of water and nutrients.

[52] The patterns of intraseasonal and interannual variability in monsoon rainfall are similar to each other [Goswami and

*Ajayamohan*, 2001,] since the seasonal mean monsoon rainfall is made up of ISOs. The integration of environmental forcing by the ecosystem confounds the rainfall, PAR, and temperature forcing and removes such a signature although there is a clear coherent variability between ISOs in monsoon rainfall and CO<sub>2</sub> fluxes. The reliance of our analysis on the CASA and VISIT models is unavoidable since observational data do not allow for the separation of temperature and rainfall effects. Models clearly tend to be deficient and the impact of model sensitivities cannot be quantified here. We do expect that our analyses will serve as basis for model intercomparisons and also direct data gathering effects to further understand some of the interesting and counterintuitive outcomes of our analyses.

#### 4.1. Possible Uncertainties in the Results

[53] Few possible sources of uncertainties in our results must be noted here. The results based on CT data shown here are merely based on the CASA model simulations and to some extent the weekly biases of NEE (subdivided into 11 ecosystem types) are reduced within the CT-assimilation system (see introduction). This guarantees that the variability discussed here is bias-corrected at least on a weekly basis and therefore the 20–60 day variability extracted here is robust. However, as mentioned in section 2, a questionable point is how much the CT data utilized the atmospheric CO<sub>2</sub> data to constrain NEE over India. CT data include little data from Indian region to constrain the NEE. Therefore, NEE over the Indian region mainly relies on the CASA derived fluxes. This limitation should be kept in mind while interpreting the results. The only possible constraint that might have entered the NEE over Indian region would be based on atmospheric CO<sub>2</sub> data from the neighboring stations. This is explained in section 2.

[54] The additional analysis of VISIT fluxes shows that the results are robust between the two products. One should remember that these two models (CASA and VISIT) employ different complexities in the process modeling of ecosystem NEE. Even with different schemes, we could obtain the ISO variability of CO<sub>2</sub> that is quite robust in both models. However, partitioning the NEE variability into NPP and RE is not free from methodological biases [*Reichstein et al.*, 2005]. For example, the CASA may miss the huge spike or pulse in respiration following rain. This is an issue which needs further attention in semi-arid ecosystems, like those regions that span in parts of India. These rain induced spikes may account for 10% of annual carbon cycling [*Xu et al.*, 2004] and are expected to be short lived but prominent following the first rain spells of the monsoon. Subsequent rains will not produce large pulses in respiration. Therefore, comparisons with observed NEE (based on eddy covariance methods) must be used to validate the model results shown here. At present there is no such data set available from India but will be available in near future as India is setting up tower-based observations of CO<sub>2</sub> and other boundary layer parameters in various parts of the country [V. K. Dadhwal, NRSC, Hyderabad, India, personal communication, 2011]. The need for eddy covariance method is highly relevant in the context of both the validation of model results and its application in carbon flux inversion [*Chevallier et al.*, 2012]. Another source of uncertainty can be the relationship between NPP, RE, and Q<sub>10</sub> used in the methods, which are

subject to vary according to different vegetation types [*Goudriaan et al.*, 2001]. *Smith and Dukes* [2012] pointed out the short-term responses of plant NEE to temperature are modified by photosynthetic and respiratory acclimation as well as biogeochemical feedback. Therefore, ISO variability of NEE may be better represented in models with such acclimation processes included.

#### 5. Summary

[55] Here, we summarize the major findings of this study: (a) the terrestrial biospheric CO<sub>2</sub> fluxes over India exhibit a significant (close to 20% of the seasonal amplitude) intraseasonal oscillation associated with a variability of monsoon rainfall; (b) a 30–60 day mode variability in CO<sub>2</sub> fluxes is larger in amplitude than the 10–20 day mode; (c) ~60 day periodicity is a preferred scale of CO<sub>2</sub> flux variability (spatially homogenous) during a dry monsoon year whereas 20–30 day periodicity is preferred (spatially inhomogeneous) during a wet monsoon year; (d) in a break (active) phase, a decrease (increase) in rainfall is associated with an increase in CO<sub>2</sub> sink (source); (e) the mechanism of CO<sub>2</sub> response with rainfall ISOs is explained as the effect of PAR shielding by organized clouds during active phase and surplus of PAR due to the absence of cloud during break phase together with the sudden possible surges in soil respirations during rain bursts in the active periods; (f) there are coherent structures of CO<sub>2</sub> flux, rainfall, and air-temperature on ISO time scale with CO<sub>2</sub> lagging the rainfall by 2–3 days and with air-temperature lagging by 3–4 days during a break monsoon phase; (g) during the active monsoon phase the lag of the latter is reduced to 2–3 days; and (h) the lag of CO<sub>2</sub> and rainfall relations is interpreted as induced by the effects of lags with air-temperature. These results are confirmed with two data sets. The study, for the first time, offers a mechanistic point of view of terrestrial biospheric CO<sub>2</sub> fluxes over India and monsoon rainfall on ISO time scales. In light of the role of ecosystem carbon dynamics on climate feedback [*Heimann and Reichstein*, 2008] and projected increase in crop yields in a high CO<sub>2</sub> environment [*Long et al.*, 2006a, 2006b], such intrinsic variability of Indian terrestrial biosphere fluxes on ISO time scales deserves more experimental research. Our study is but a first step in this direction.

[56] However, we offer a cautionary note that the variability of biospheric fluxes on intraseasonal time scales is based mostly on prior first-guess-flux estimates (from CASA). To some extent, we tried to boost the confidence in our findings by analyzing the VISIT fluxes as well. Therefore, new simulations that incorporate CO<sub>2</sub> observations from the Indian subcontinent in the CT may lead to improvements in the representations of CO<sub>2</sub> intraseasonal variability over the region.

[57] **Acknowledgment.** Carbon Tracker 2010 results are provided by NOAA ESRL, Boulder, Colorado, USA, from the website at <http://www.esrl.noaa.gov/gmd/ccgg/carbontracker/tutorial.html>. VV thanks Saito Makato, LSCE, France, for initial discussions. SM is supported by carbon cycle program at NIES, Japan. RM thanks the generous support of IITM and gratefully acknowledges the NASA PO Biophysical Feedback grant and the ONR DYNAMO grant. APHRODITE data are taken from <http://www.chikyu.ac.jp/precip/index.html>. ECMWF ERA-Interim data used in this study have been obtained from the ECMWF data server. NDVI data are obtained from <http://jisao.washington.edu/data/ndvi/#data>. GLCC data sets are obtained from <http://edcdaac.usgs.gov/glcc/glcc.html>.

Yosuke Niwa, MRI, Tsukuba, Japan, is thanked for kindly providing us the CONTRAIL inversion fluxes for South Asia.

## References

- Atkin, O. K., et al. (2008), Using temperature-dependent changes in leaf scaling relationships to quantitatively account for thermal acclimation of respiration in a coupled global climate-vegetation model, *Glob. Chang. Biol.*, *14*, 2709–2726.
- Atkin, O. K., C. Holly, and M. C. Ball (2000), Acclimation of snow gum (*Eucalyptus pauciflora*) leaf respiration to seasonal and diurnal variations in temperature: The importance of changes in the capacity and temperature sensitivity of respiration, *Plant Cell Environ.*, *23*, 15–26.
- Braswell, B. H., D. S. Schimel, E. Linder, and B. Moore (1997), The response of global terrestrial ecosystems to interannual temperature variability, *Science*, *278*, 870–872.
- Canadell, J. G., et al. (2007) Contributions to accelerating atmospheric CO<sub>2</sub> growth from economic activity, carbon intensity, and efficiency of natural sinks, *Proceedings of National Academy of Science*, *104*, 41, 18,866–18,870.
- Ciais, P., et al. (2005), Europe-wide reduction in primary productivity caused by the heat and drought in 2003, *Nature*, *437*(22), 529–533.
- Chevallier, F., et al. (2012), What eddy-covariance measurements tell us about prior land flux errors in CO<sub>2</sub>-flux inversion schemes, *Global Biogeochem. Cycles*, *26*, GB1021, doi:10.1029/2010GB003974.
- Dee, D. P., et al. (2011), The ERA-Interim reanalysis: Configuration and performance of the data assimilation system, *Quart. J. R. Meteorol. Soc.*, *137*, 553–597, doi:10.1002/qj.828.
- Field, C. B., J. T. Randerson, and C. M. Malmstrom (1995), Global net primary production—Combining ecology and remote-sensing, *Remote Sens. Environ.*, *51*, 74–88.
- Friedl, M. A., et al. (2002), Global land cover mapping from MODIS: Algorithms and early results, *Remote Sens. Environ.*, *83*, 287–302.
- Gadgil S., and K. Rupa Kumar (2006), The Asian monsoon—Agriculture and economy. The Asian monsoon. 651–683.
- Goudriaan, J., J. J. R. Groot, and P. W. J. Uithol (2001), *Terrestrial Global Productivity*, edited by B. Saugier and J. Roy, Academic Press, San Diego, Calif.
- Goswami B. N., and R. S. Ajayamohan (2001), Intraseasonal oscillations and interannual variability of the Indian summer monsoon, *J. Climate*, *14*(6), 1180–1198.
- Goswami, B. N. (2005), South Asian summer monsoon: An overview in *The Global Monsoon System: Research and Forecast*, Eds. C.-P. Chang, B. Wang, N.-C. G. Lau, Chapter 5, pp 47, WMO (World Meteorological Organization)/TD no. 1266.
- Gurney, K. R., R. M. Law, A. S. Denning, P. J. Rayner, B. C. Pak, D. Baker, P. Bousquet, L. Bruhwiler, Y. H. Chen, and P. Ciais (2004), Transcom 3 inversion intercomparison: Model mean results for the estimation of seasonal carbon sources and sinks, *Global Biogeochem. Cycles*, *18*(1), GB1010, doi:10.1029/2003GB002111.
- Heimann, M., and M. Reichstein (2008), Terrestrial ecosystem carbon dynamics and climate feedbacks, *Nature*, *451*, 289–292, doi:10.1038/nature06591.
- ISFR (2011), India state of forest report, forest survey of India, Ministry of Environment and Forest, Government of India, [http://fsi.org.in/sfr\\_2011.htm](http://fsi.org.in/sfr_2011.htm).
- Ito, A. (2010), Changing ecophysiological processes and carbon budget in East Asian ecosystems under near-future changes in climate: Implications for long-term monitoring from a process-based model, *J. Plant Res.*, *123*, 577–588.
- Jin, D., R. Murtugudde, and D. E. Waliser (2012), Tropical Indo-Pacific Ocean chlorophyll response to MJO forcing, *J. Geophys. Res.*, *117*, C11008, doi:10.1029/2012JC008015.
- Krishnamurti, T. N., and P. Ardanuy (1980), The 10–20-day westward propagating mode and breaks in the monsoons, *Tellus*, *32*, 15–26.
- Krishnamurti, T. N., and D. Subrahmanyam (1982), The 30–50 day mode at 850 mb during MONEX, *J. Atmos. Sci.*, *39*, 2088–2095.
- Krishnan, R., C. Zhang, and M. Sugi (2000), Dynamics of breaks in the Indian summer monsoon, *J. Atmos. Sci.*, *57*, 1354–1372.
- Krishnamurthy, V., and J. Shukla (2000), Intraseasonal and interannual variability of rainfall over India, *J. Climate*, *13*, 4366–4377.
- Lau, K. M., and L. Peng (1987), Origin of low-frequency (intraseasonal) oscillations in the tropical atmosphere. Part I: Basic theory, *J. Atmos. Sci.*, *44*, 950–972.
- Lal, M., and R. Singh (2000), Carbon sequestration potential of Indian forests, *Environ. Monit. Assess.*, *60*(3), 315–327.
- Long, S. P., E. A. Ainsworth, A. D. B. Leakey, J. Nösberger, and D. R. Ort (2006a), Food for thought: Lower-than-expected crop yield stimulation with rising CO<sub>2</sub> concentrations, *Science* 30 June 2006: 312(5782) pp. 1918–1921, doi:10.1126/science.1114722.
- Long, S. P., S. Xin-GuangZhui L. Naidu, and D. R. Ort (2006b), Can improvement in photosynthesis increase crop yields?, *Plant Cell Environ.* (2006), *29*, 315–330.
- Mahecha, M. D., et al. (2010), Global convergence in the temperature sensitivity of respiration at ecosystem level, *Science*, *329*, 838–840.
- Maksyutov, S., et al. (2012), Regional CO<sub>2</sub> flux estimates for 2009–2010 based on GOSAT and ground-based CO<sub>2</sub> observations, *Atmos. Chem. Phys. Discuss.*, *12*, 29,235–29,288, doi:10.5194/acpd-12-29235-2012.
- Mooley, D., and J. Shukla (1987), Variability and forecasting of the summer monsoon rainfall over India, in *Monsoon Meteorology*, edited by C. P. Chang, and T. N. Krishnamurti, pp. 26–59, Oxford University Press.
- Mooley, D. A., and B. Parthasarathy (1984), Fluctuations in all-India summer monsoon rainfall during 1871–1978, *Clim. Chang.*, *6*(3), 287–301.
- Murakami, T., T. Nakazawa, and J. He (1984), On the 40–50 day oscillations during the 1979 Northern Hemisphere summer. I: Phase propagation. *J. Meteorol. Soc. Jap.*, *62*, 440–468.
- Nayak, R. K., N. R. Patel, and V. K. Dadhwal (2010), Estimation and analysis of terrestrial net primary productivity over India by remote-sensing-driven terrestrial biosphere model, *Environ Monit. Assess.*, *170*(1–4), 195–213, doi:10.1007/s10661-00-1226-9.
- Nayak, R. K., N. R. Patel, and V. K. Dadhwal (2013), Inter-annual variability and climate control of terrestrial net primary productivity over India, *Int. J. Climatol.* *33*, 132–142, doi:10.1002/joc.3414.
- Niwa, Y., T. Machida, Y. Sawa, H. Matsuuda, T. J. Schuck, C. A. M. Brenninkmeijer, R. Imasu, and M. Satoh (2012), Imposing strong constraints on tropical terrestrial CO<sub>2</sub> fluxes using passenger aircraft-based measurements, *J. Geophys. Res.*, *117*, D11303, doi:10.1029/2012JD017474.
- Onogi, K., et al. (2007), The JRA-25 reanalysis, *J. Meteorol. Soc. Jap.*, *85*, 369. Jap.
- Parthasarathy, B. (1984), Interannual and long-term variability of Indian summer monsoon rainfall, *Proc. Indian Acad. Sci (Earth Planet. Sci.)*, *93*, 371–385.
- Parthasarathy, B., A. A. Munot, and D. R. Kotawale, (1988): Regression model for estimation of Indian food grain production from summer monsoon rainfall, *Agr. Forest. Meteorol.*, *42*(2–3), March 1988, Pages 167–182.
- Peters, W., et al. (2007), An atmospheric perspective on North American carbon dioxide exchange: Carbon Tracker, *Proc. National. Aca. Science*, November 27, 2007, *104*(48), 18,925–18,930.
- Pillai, P. A., and A. K. Sahai (2012), Moist dynamics of active/break cycle of Indian summer monsoon rainfall from NCEP 2nd MERRA reanalysis (revised, Climate Dynamics).
- Preethi, B., and V. Revadekar (2012), Kharif food grain yield and daily summer monsoon precipitation over India, *International Journal of Climatology*, doi:10.1002/joc.3565.
- Potter, C. S., S. A. Klooster, R. B. Myneni, V. Genovese, P. N. Tan, and V. Kumar (2003), Continental scale comparisons of terrestrial carbon sinks estimated from satellite data and ecosystem modeling, 1982–1998, *Global Planetary Change*, *39*, 201–213.
- Rajeevan, M., S. Gadgil, and J. Bhate (2010), Active and break phase of Indian summer monsoon, *Journal of Earth System Sciences*, *119*, 229–247.
- Randerson, J. T., M. V. Thompson, C. M. Malmstrom, C. B. Field, and I. Y. Fung (1996), Substrate limitations for heterotrophs: Implications for models that estimate the seasonal cycle of atmospheric CO<sub>2</sub>, *Global Biogeochem. Cycles*, *10*, 585–602.
- Reichstein, M., et al. (2005), On the separation of net ecosystem exchange into assimilation and ecosystem respiration: Review and improved algorithm, *Glob. Chang. Biol.*, *11*, 1424–1439, doi:10.1111/j.1365-2486.2005.001002.x.
- Raupach, M. R. (2011), Carbon cycle: Pinning down the land carbon sink, *Nature Climate Change*, *1*, 148–149.
- Saito, M., A. Ito, and S. Maksyutov (2011), Evaluation of biases in JRA-25/JCDAS precipitation and their impact on the global terrestrial carbon balance, *J. Climate*, *24*, 4109–4125.
- Sikka, D. R., and S. Gadgil (1980), On the maximum cloud zone and ITCZ over the Indian longitudes during the southwest monsoon, *Mon. Wea. Rev.*, *108*, 1122–1135.
- Smith, N. G., and J. S. Dukes (2012), Plant respiration and photosynthesis in global-scale vegetation models: Incorporating acclimation to temperature and CO<sub>2</sub>, *Glob. Chang. Biol.*, doi:10.1111/j.1365-2486.2012.02797.x.
- Simmons, A., S. Uppala, D. Dee, and S. Kobayashi, (2007), ERA-Interim: New ECMWF reanalysis products from 1989 onwards. Newsletter 110—Winter 2006/07, ECMWF, 11 pp.
- Tian, H., J. M. Melillo, D. W. Kicklighter, S. Pan, J. Liu, A. D. McGuire, and B. Moore III, (2003), Regional carbon dynamics in monsoon Asia and its implications for the global carbon cycle, *Global and Planetary Change*, *37*, 201–217.
- Tiwari, Y. K., V. Valsala, R. Vellore, and R. K. Kunchala (2013), Assessment of the potential usefulness of two surface CO<sub>2</sub> monitoring stations over

- India using Lagrangian transport modeling, *Climate Change Research*, in press.
- van der Werf, G. R., J. T. Randerson, G. J. Collatz, and L. Giglio (2003), Carbon emissions from fires in tropical and subtropical ecosystems, *Glob. Chang. Biol.*, *9*, 547–562.
- van der Werf, G. R., J. T. Randerson, L. Giglio, G. J. Collatz, P. S. Kasibhatla, and A. F. Arellano Jr. (2006), Interannual variability in global biomass burning emissions from 1997 to 2004, *Atmos. Chem. Phys.*, *6*, 3423–3441.
- Valsala V., and M. Ikeda (2005), An extreme drought event in the 2002 summer monsoon rainfall and its mechanisms proved with a moisture flux analysis, *Scientific Online Letters on the Atmosphere*, *1*, 173–176.
- Waliser, D. E., R. Murtugudde, P. Strutton, and J.-L. Li (2005), Sub-seasonal organization of ocean chlorophyll: Prospects for prediction based on the Madden-Julian oscillation, *Geoph. Res. Lett.*, *32*(23), L23602, doi:10.1029/2005GL024300.
- Wu, Z., P. Dijkstra, G. W. Koch, J. Penuelas, and B. A. Hungate (2011), Responses of terrestrial ecosystems to temperature and precipitation change: A meta-analysis of experimental manipulation, *Glob. Chang. Biol.*, *17*, 927–942, doi:10.1111/j.1365-2486.2010.02302.x.
- Xu, L., D. D. Baldocchi, and J. Tang (2004), How soil moisture, rain pulses, and growth alter the response of ecosystem respiration to temperature, *Global Biogeochem. Cycles*, *18*, GB4002, doi:10.1029/2004GB002281.
- Yasunari, T. (1979), Cloudiness fluctuation associated with the Northern Hemisphere summer monsoon, *J. Meteorol. Soc. Jap.*, *57*, 227–242.
- Yasunari, T. (1980), A quasi-stationary appearance of 30–40 day period in the cloudiness fluctuations during the summer monsoon over India, *J. Meteorol. Soc. Jap.*, *58*, 225–229.
- Yatagai, A., O. Arakawa, K. Kamiguchi, H. Kawamoto, M. I. Nodzu, and A. Hamada (2009), A 44-year daily gridded precipitation dataset for Asia based on a dense network of rain gauges, *SOLA*, *5*, 137–140, doi:10.2151/sola.2009-035.